We get technical

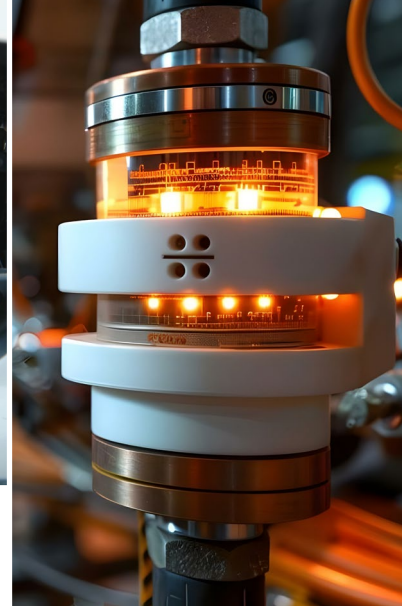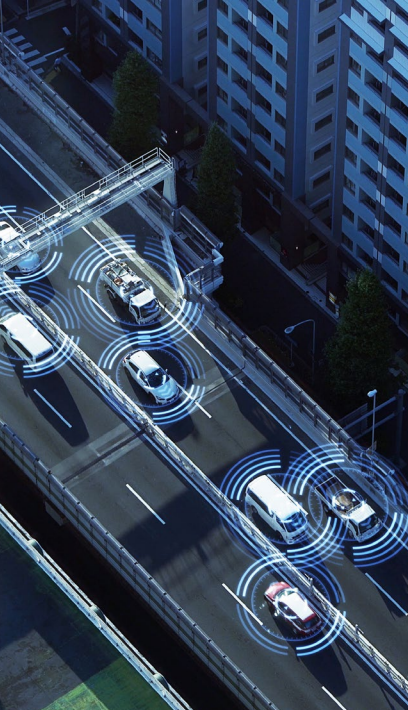Wide bandgap semiconductors are reshaping the transportation world

How to use residual current monitors to ensure electrical safety when charging electric vehicles

AEC-Q200 qualified fuses play a critical role in the automotive environment

Reduce EV range anxiety and improve safety using integrated FOC motor control and advanced sensors

DigiKey

contents

Editor's note

In today's rapidly changing world of transportation, exciting new technologies are transforming how we move. Wide bandgap semiconductors are making electricvehicles more efficient and powerful, while LiDAR technology is bringing us closer to the reality of self-driving cars by improving navigation and safety. As morepeople turn to electric vehicles, sensors play an essential role in keeping the charging process safe and reliable. Automotive security is also getting a boost fromAEC-Q200 standards, ensuring that vehicles can handle even the toughest conditions. Tackling electric vehicle range anxiety is another key step in making thesecars safer and more appealing, and CAN bus systems help keep everything running smoothly behind the scenes. Together, these innovations are shaping a smarter,safer future for everyone on the road.

Wide bandgap semiconductors are reshaping the transportation world

By Rolf Horn
Contributed By DigiKey's
North American Editors

The entire transportation sector is undergoing a radical transformation, with internal combustion engine (ICE) vehicles gradually giving way to less polluting electric and hybrid cars and cleaner mass transportation solutions (trains, aircraft, and ships). Solutions capable of maximizing efficiency and reducing environmental impact are needed to contain greenhouse gases (GHG) emissions and mitigate global warming.

Wide bandgap (WBG) semiconductors exhibit several properties that make them attractive for transportation applications. Their usage can result in more efficient, faster, and lightweight vehicles with improved range and reduced environmental impact.

Property	SI	SIC	GAN
Bandgap energy (eV)	1.1	3.2	3.4
Breakdown electric field (MV/cm²)	0.3	3.5	3.3
Electron mobility (cm²/V•s)	1500	900	900-2000
Electron saturation velocity (cm/s)	$1 \cdot 10^7$	$2.2 \cdot 10^7$	$2.5 \cdot 10^7$
Thermal conductivity (W/cm•K)	1.5	5.0	1.3
Dielectric constant	11.8	10	8.9

Table 1: Comparison of the properties of Si, SiC, and GaN.

Properties of WBG materials

Wide bandgap materials are quickly transforming the power electronics area due to their advantages over commonly used silicon (Si). While silicon has a bandgap of 1.1 electronvolts (eV), WBG materials have a bandgap of 2 to 4 eV. Additionally, the breakdown electric field of most WBG semiconductors is substantially higher than silicon. That means they can operate at significantly higher temperatures and voltages, providing higher power levels and lower losses.

Table 1 lists the main properties of silicon carbide (SiC) and gallium nitride (GaN), the two most popular WBG materials, compared to silicon.

The main advantages of SiC power devices, compared to silicon-based counterparts, are the following:

- Low switching losses: SiC MOSFETs are unipolar devices that exhibit very low turn-on and turn-off switching losses. This property enables higher switching frequencies with lower losses, allowing the reduction of passive components and magnetics

- Low conduction losses: due to the absence of a bipolar junction, SiC devices can also reduce losses during light-load or partial-load operation

- High operating temperatures: silicon carbide offers superior thermal properties compared to silicon. SiC exhibits low leakage currents over a wide range of temperatures, allowing operation beyond 200°C. Simplified cooling and excellent thermal management are a consequence of this property

- Intrinsic body diode: thanks to this characteristic, SiC MOSFETs can operate in diode mode in the third quadrant providing excellent performance in power applications

Combining the above properties allows obtaining SiC devices with higher power density, efficiency, operational frequencies, and smaller footprint.

The main advantages of [GaN power devices](), compared to Si and SiC counterparts, are the following:

- GaN devices can operate in the third quadrant without reverse recovery charge even though they do not have an intrinsic body diode. As a result, there is no need for an anti-parallel diode

- Low gate charge QG and on-resistance RDS(ON), which translate into lower drive losses and faster switching rates

- Zero reverse recovery, resulting in lower switching losses and less EMI noise

- High dv/dt: GaN can switch at very high frequencies and has 4x faster turn-on and 2x faster turn-off than SiC MOSFETs with similar RDS(ON)

Applications of WBG devices

As highlighted in Figure 1, there are applications where SiC and GaN offer the best performance and others where their characteristics overlap those of silicon. Often, GaN devices are the best choice for high-frequency applications, whereas SiC devices have high potential at high voltages.
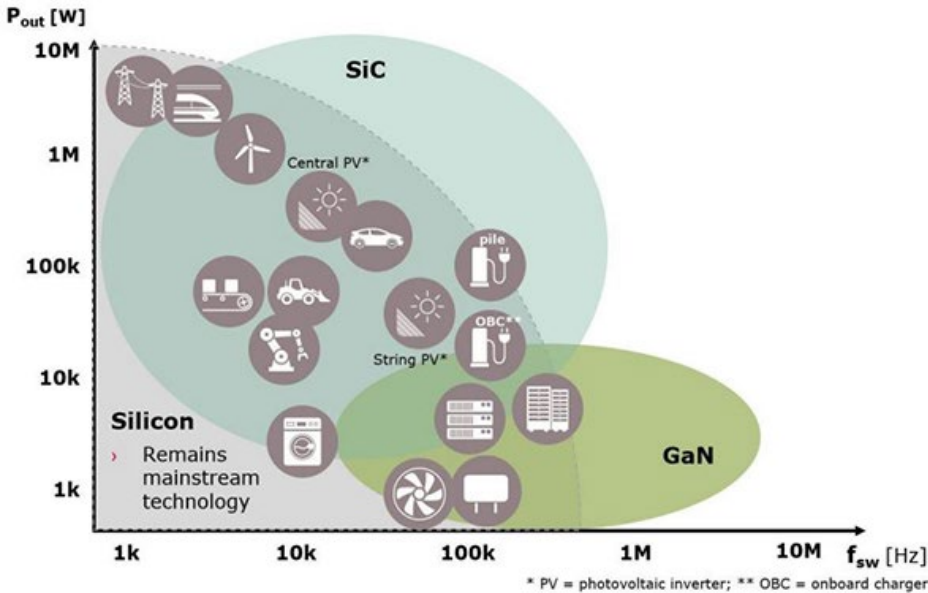

Figure 1: Potential applications of Si, SiC, and GaN devices. (Source: [Infineon]())

Hybrid and electric vehicles

H/EVs use several power electronics systems to transform grid or engine energy into a form suitable for powering motor and auxiliary devices. Most H/EVs also use regenerative braking, in which the wheels rotate the generator to charge the battery.

The traction inverter is a crucial component in these vehicles, converting the DC high voltage from the batteries into AC for powering the three-phase motor (see Figure 2). Due to the high power involved, SiC devices are preferred in this application, with a rating of 650 V or 1.2 kV, depending

on the topology of the inverter. SiC helps reduce losses, size, and weight, allowing solutions with small form factors.

The onboard charger (OBC) connects to the grid, converting AC into DC voltage to charge the battery. OBC output power is usually between 3.3 kW and 22 kW and relies on high voltage (600 V and above) power devices. While both SiC and GaN are suitable for this application, GaN's features, like high switching frequency, low conduction losses, and reduced weight and size, make it the ideal solution for implementing OBCs.
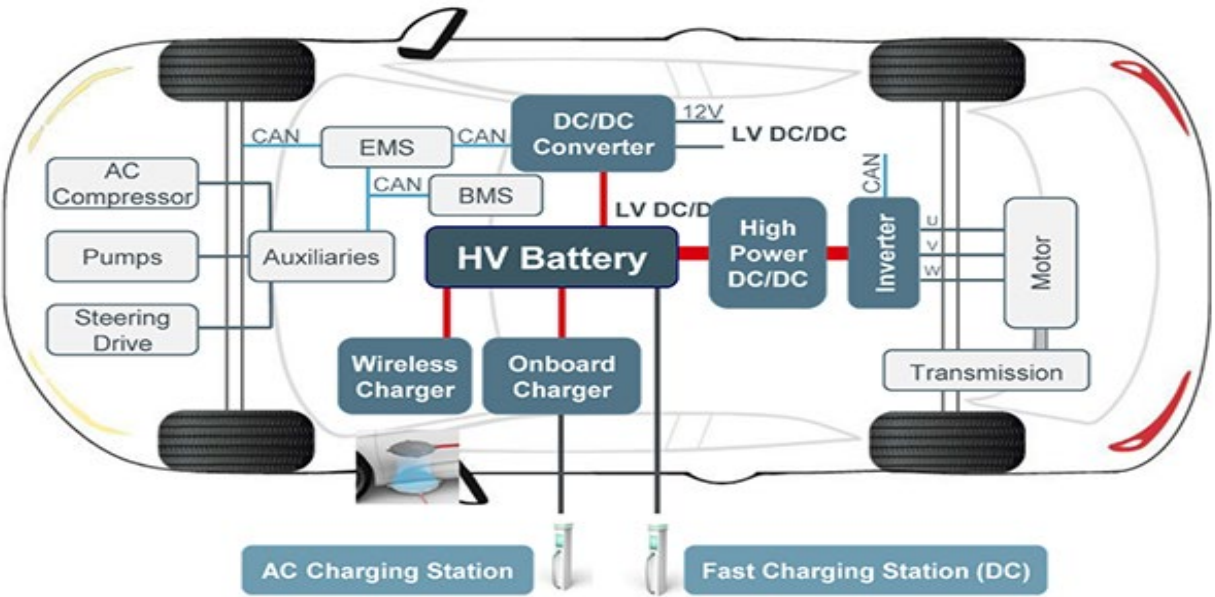

Figure 2: Main components of a H/EV. (Source: [ROHM Semiconductor]())

Type	Onboard Charger	Inverter and HV Converter	LV Converter
Power	3.3 kV >	12 kW to 400 kW	1 kW to 10 kW
Input V	120 V to 240 V	200 V to 400 V	200 V to 400 V
Output V	200 V to 400 V	100 V to 650 V	12 V to 48 V
Si efficiency	85% to 93%	83% to 95%	85% to 90%
SiC efficiency	95% to 96%	96% to 97%	96% to 99%
GaN efficiency	94% to 98%	Not Available	95% to 99%
Power device	Discrete 600 V to 900 V	Discrete/Module 600 V to 1200 V	Discrete 600 V to 900 V

Table 2: Applications of WBG in H/EVs and comparison of performance with Si.

Another application of WBG in H/EVs is the low-voltage (LV) DC-DC converter, responsible for stepping down the battery voltage (200 V in HEVs, above 400 V in EVs) to the 12 V/48 V DC voltage required for

powering the auxiliary systems. Featuring a typical power of less than 1 kW, the LV converter can achieve higher frequencies using GaN and SiC devices.

Rail transportation

Electric trains draw power from the grid via a catenary line or a third rail, converting it into a form suitable for the motors and the auxiliary systems. If the train operates on an AC line, a transformer and rectifier must step down and condition the voltage to DC. The DC voltage is then split and delivered through inverters to address the needs of the auxiliary and traction systems.

The traction inverter transforms DC into AC for powering the motors and reconditions the electricity produced by regenerative braking. Therefore, this converter is designed to run a bidirectional flow of energy. Instead, the auxiliary

inverter supplies power for cooling systems, passenger comfort, and other non-movement-related needs.

The size of the power electronics within the traction inverter depends on the class of train:

- Transit trains: 1.2 kV to 2.5 kV
- Commuter trains: 1.7 kV to 3.3 kV
- Intercity trains: above 3.3 kV

However, most trains use either 3.3 kV or 1.7 kV.

Regenerative braking, which returns a part of the electricity to the local grid, rail power distribution system, or energy storage, makes the system more complicated than those in the previously stated applications. Regenerated energy must be stored or used immediately; otherwise, it is lost.

Bipolar Si-based IGBTs and freewheeling diodes, traditionally used in power modules for railway traction applications, can be replaced by unipolar SiC-based MOSFETs and diodes, thus increasing the switching frequency and power density.

Conduction and switching losses must be decreased, and the maximum junction temperature must be raised to reduce the weight and volume of the power electronic equipment used in railway traction applications. For the widely used bipolar silicon power devices, increasing conduction losses and decreasing switching losses have the opposite effects. A unipolar device does not experience the trade-off between the conduction and switching losses as bipolar devices do. As a result, switching losses could be reduced while minimizing conduction losses.

Power losses in the electric rail can be drastically reduced with WBG power electronics. As a result, less energy will be drawn from the grid, and more will be returned via regenerative braking. WBG devices also offer additional benefits that considerably help rail transportation in addition to efficiency increases, such as:

- Reduced weight has significant impacts on efficiency
- Higher operating temperature allows for a smaller cooling system
- Increased switching frequency enables smaller passive dimensions, which lowers the weight of the traction and auxiliary inverters. The inverter and motor can respond to variations in demand more quickly thanks to the higher switching frequency, thus boosting efficiency. Finally, since the higher frequency is less audible and cooling fans may be turned off, railway stops would be less noisy when trains are present.

Marine and aviation applications

Power electronics innovations have benefited the marine sector for a long time. On the ship, medium voltage AC level electricity from synchronous generators powered by diesel engines is supplied to various loads. Propulsion drives

(a mixture of AC-DC and DC-AC converters) and other loads are primarily among them.

Recent trends in the marine sector are trying to replace AC electrical distribution networks with DC distribution networks. This solution removes the need to synchronize the generators to the AC power distribution, provided they can operate at variable speeds, and achieves fuel savings. On the other hand, it requires the introduction of rectifier circuits (AC-DC converters) between AC generators and the DC power distribution network.

Marine propulsion variable speed drives are crucial ship components that must operate with extreme reliability. They are frequently rated from a few watts to a few tens of megawatts. Often, these drives are the most significant power conversion blocks in a ship with AC electrical power distribution. Hence their great efficiency is crucial.

Once more, conventional silicon-based power devices are being replaced by SiC and GaN devices, which increase efficiency while reducing size and weight. WBG devices will soon overtake Si-based devices as the industry leader, bringing cutting-edge power electronics system solutions that are impossible with silicon technology.

Future fuel-turbine-powered electrical generators will be the prime mover for hybrid and all-

electric avionic propulsion systems. Power electronics will subsequently be used to connect the generator and motor. Very high DC voltage buses are necessary to ensure enough power can be available. These buses can range in voltage from a few kVs for light vehicles to the MV range for airplanes. Moreover, a high DC voltage bus makes it possible to use permanent magnet synchronous machines as generators, which lowers reactive power and the power electronics' rating. The power converters need equipment that can function at high switching frequencies due to the fast generator rotational speed, which results in smaller and lighter filter elements.

Silicon carbide is the most promising semiconductor device to meet all requirements while ensuring high conversion efficiency. For aircraft in the lower power range, newly created 3.3 kV and 6.5 kV SiC MOSFET devices are of significant interest. They can also be employed in modular power converter topologies to meet larger aircraft's higher voltage/power requirements.

Conclusion

Wide bandgap semiconductors, such as silicon carbide (SiC) and gallium nitride (GaN), offer several advantages over traditional semiconductors in their ability to handle high voltages and

temperatures with lower power loss. These characteristics make them particularly well-suited for power electronics used in various applications, including transportation.

WBG semiconductors are used in the transportation industry to develop more efficient and reliable electric and hybrid vehicles. The lower power loss of wide bandgap semiconductors allows higher switching frequencies, reducing power electronics' size and weight. This, in turn, can result in greater vehicle range, faster charging times, and improved overall performance.

Wide bandgap semiconductors also enable the development of more compact and efficient powertrains, including motor drives and inverters for EVs and HEVs. By reducing the size and weight of these components, vehicle designers can free up space for other components or improve the vehicle's overall aerodynamics.

In addition to electric and hybrid electric vehicles, wide bandgap semiconductors are also used in other transportation forms, such as airplanes and trains. In these applications, the high temperature and high voltage capabilities of wide bandgap semiconductors can improve the efficiency and reliability of power electronics, leading to reduced operating costs and improved safety.
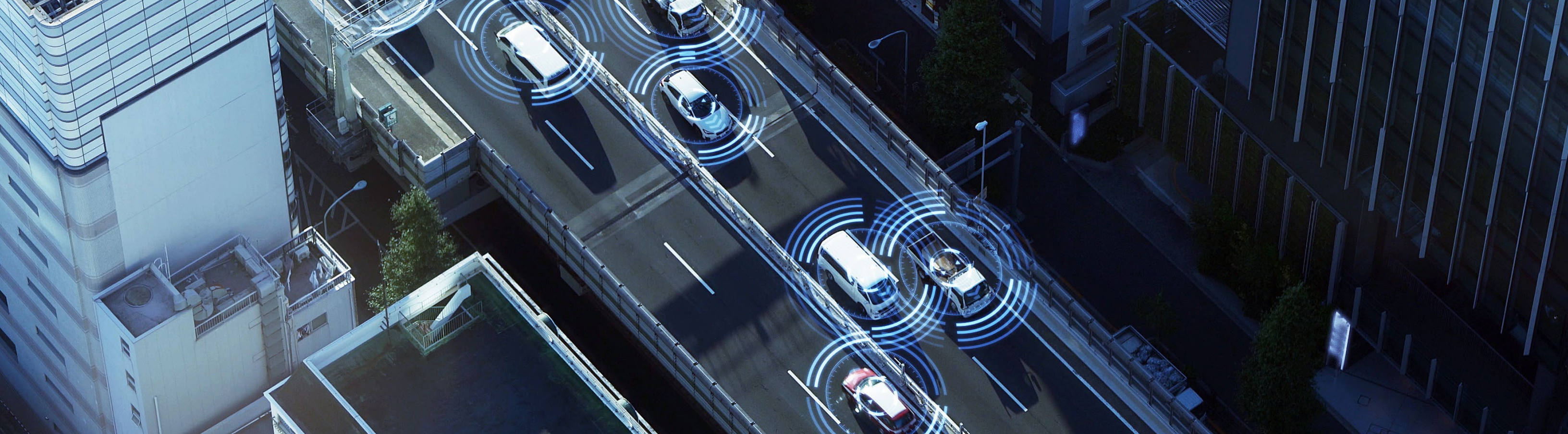
Quick guide to GaN FETs for LiDAR in autonomous vehicles

By Kenton Williston
Contributed By DigiKey's
North American Editors

Light detection and ranging (LiDAR) applications include autonomous vehicles, drones, warehouse automation, and precision agriculture. Humans are present in most of these applications, leading to concerns about a LiDAR laser's potential to cause eye damage. To prevent injury, automotive LiDAR systems must meet IEC 60825-1 Class 1 safety requirements while transmitting at up to 200 watts.

The general solution uses a pulse of 1 to 2 nanoseconds (ns) at a 1 to 2 megahertz (MHz) repetition rate. This is challenging as a microcontroller or other large digital integrated circuit (IC) is needed to control the laser diode but cannot directly drive it, so a gate driver circuit must be added. Also, this gate driver design must be optimized to ensure that the performance of the LiDAR system is suitable for Society of Automotive Engineers (SAE) Level 3 and higher advanced driver assistance (ADAS) systems.

Designing a high-power and high-performance gate driver that meets the safety requirements of IEC 60825-1 using discrete components is complex and time consuming, potentially adding to cost and extending time to market. To meet these challenges, designers can turn to integrated, high-speed gate driver ICs paired with gallium nitride (GaN) power field effect transistors (FETs). Using an integrated solution minimizes the parasitics that degrade the integrity of the drive signal, particularly in the high-current laser power loop, and it enables locating the high-current driver close to the power switches, minimizing the effect of high-frequency switching noise.

This article provides a brief introduction to LiDAR. It discusses applications and safety requirements before reviewing the challenges of designing automotive LiDAR, focusing on the high-current laser power loop. It then presents LiDAR solutions from Efficient Power Conversion (EPC), Excelitas Technologies, ams OSRAM, and Texas Instruments, including GaN power FETs, gate drivers, and laser diodes, along with evaluation boards and implementation guidance to speed the development process.

How LiDAR works

LiDAR systems measure the round-trip time-of-flight (ToF) (Δt) of a laser beam pulse to calculate the distance from an object (Figure 1). The distance (d) can be calculated using the formula $d = c * \Delta t/2$, where c is the speed of light in air. Short pulse durations are one of the keys to LiDAR. Given that the speed of light is approximately 30 centimeters per ns (cm/ns), a 1 ns LiDAR pulse has a length of about 30 cm. This puts a lower limit of about 15 cm on the minimum feature size that can be resolved. As a result, LiDAR pulses must be limited to a few nanoseconds to have a useful resolution for human-scale environments.
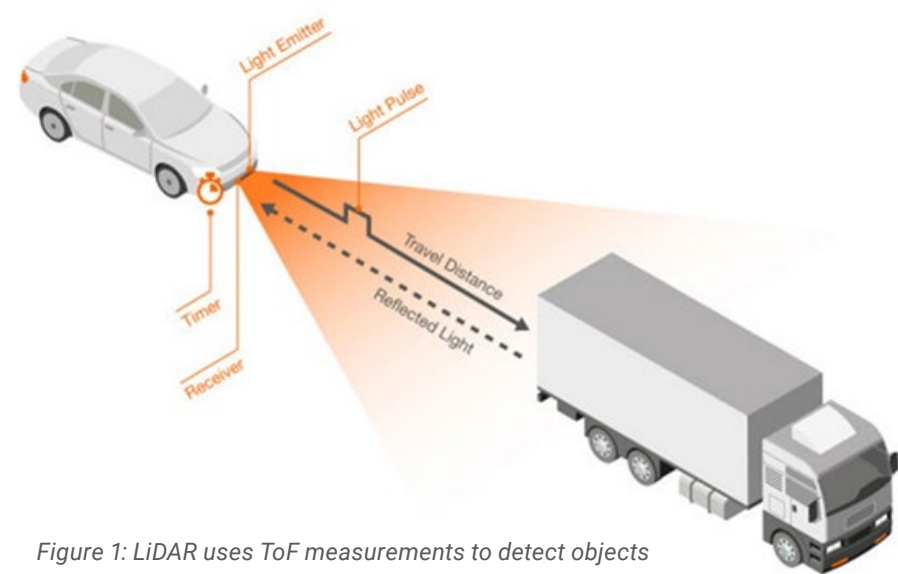
Figure 1: LiDAR uses ToF measurements to detect objects and determine their distance. (Image source: ams OSRAM)
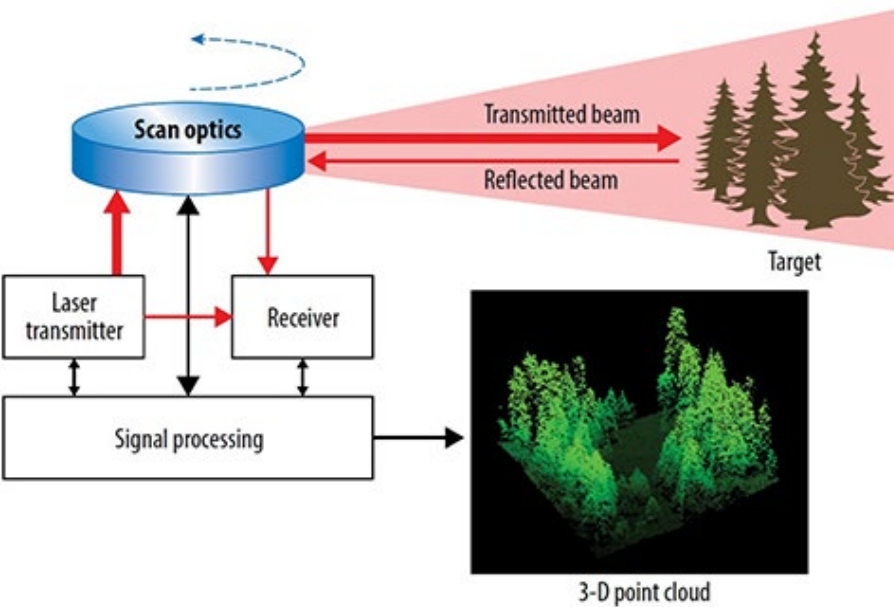

Figure 2: LiDAR systems combine large numbers of ToF measurements to create 3-D point clouds and images of a target area. (Image source: EPC)

Pulse width, peak power, repetition frequency, and duty cycle are primary LiDAR specifications. For example, a typical laser diode used in a LiDAR system may have a pulse width of 100 ns or less, a peak power of >100 watts, a 1 kilohertz (kHz) or higher repetition frequency, and a duty cycle of 0.2%. The higher the peak power, the longer the detection range of the LiDAR, but thermal dissipation is a tradeoff. For a pulse width of 100 ns, the average duty cycle is usually limited to 0.1% to 0.2% to prevent laser overheating. Shorter pulse widths also contribute to LiDAR safety.

IEC 60825-1 defines laser safety in terms of the maximum permissible exposure (MPE), which is the highest energy density or power of a light source with negligible potential to cause eye damage. To be negligible, the MPE power level is limited to roughly 10% of the energy density, which has a 50% possibility of causing eye damage. With a constant power level, shorter pulse widths have a lower average energy density and are safer.

While a single LiDAR ToF measurement can determine the distance to an object, thousands or millions of LiDAR ToF measurements can be used to create a three-dimensional (3-D) point cloud (Figure 2).

A point cloud is a collection of data points storing large amounts of information called components. Each component contains a value describing an attribute. The components may include x, y, and z coordinates and information about the intensity, color, and time (to measure object movement). LiDAR point clouds create a real-time 3-D model of the target area.

Use GaN FETs to power LiDAR lasers

GaN FETs switch much faster than their silicon counterparts, making them suitable for LiDAR applications requiring very narrow pulse widths. For example, the EPC2252 from EPC is an AEC-Q101 automotive-qualified 80 volt GaN FET capable of current pulses up to 75 amperes (A) (Figure 3). The EPC2252 has a maximum on resistance (RDS(on)) of 11 milliohms (mΩ), a maximum total gate charge (Qg) of 4.3 nanocoulombs (nC), and zero source-drain recovery charge (QRR).
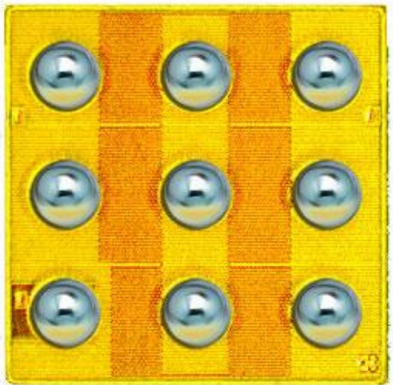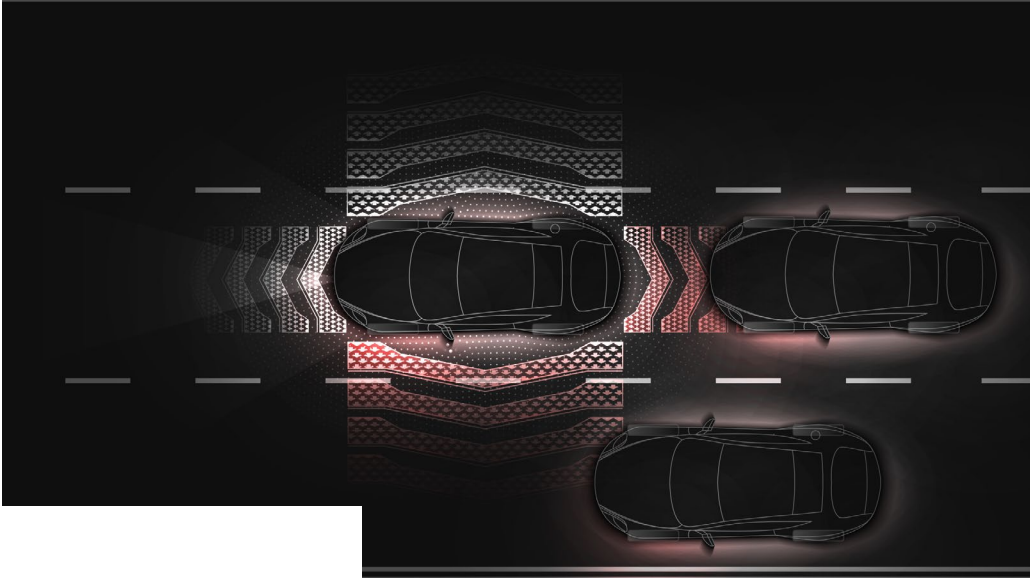

Figure 3: The EPC2252 GaN FET is AEC-Q101 qualified and is suitable for driving laser diodes in automotive LiDAR systems. (Image source: EPC)

The IC is delivered as a die-size ball grid array (DSBGA). This means the passivated die is directly attached to solder balls without any other packaging. As a result, the DSBGA chips are the same size as the silicon die, minimizing their form factor. In this case, the EPC2252 uses a 9-DSBGA implementation that measures 1.5 x 1.5 millimeters (mm). It has a thermal resistance of 8.3°C per watt (°C/W) from junction to board, making it suitable for high-density systems.

Designers can use EPC's EPC9179 development board for a fast start by employing the EPC2252 in LiDAR systems with total pulse widths of 2 to 3 ns (Figure 4). The EPC9179 includes an LMG1020 gate driver from Texas Instruments that can be controlled by an external signal or an onboard narrow-pulse generator (with sub-nanosecond precision).
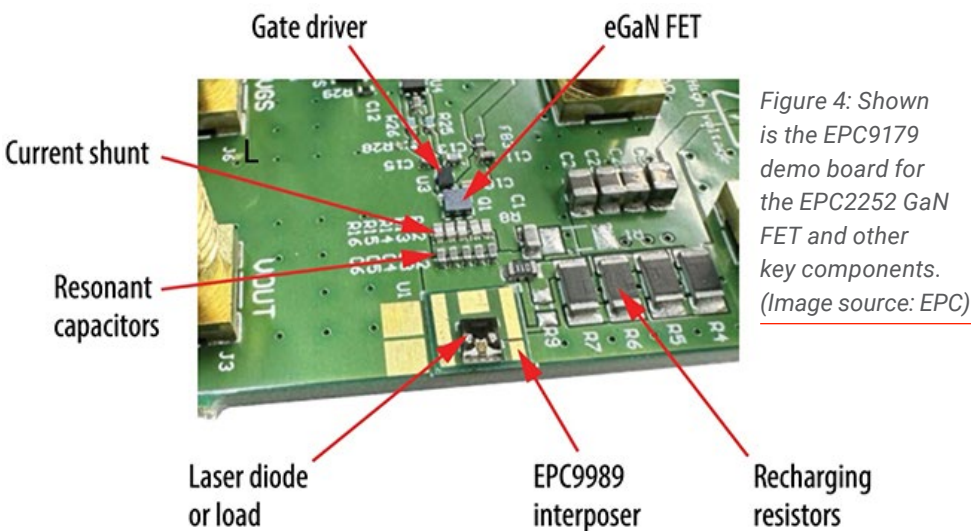

Figure 4: Shown is the EPC9179 demo board for the EPC2252 GaN FET and other key components. (Image source: EPC)
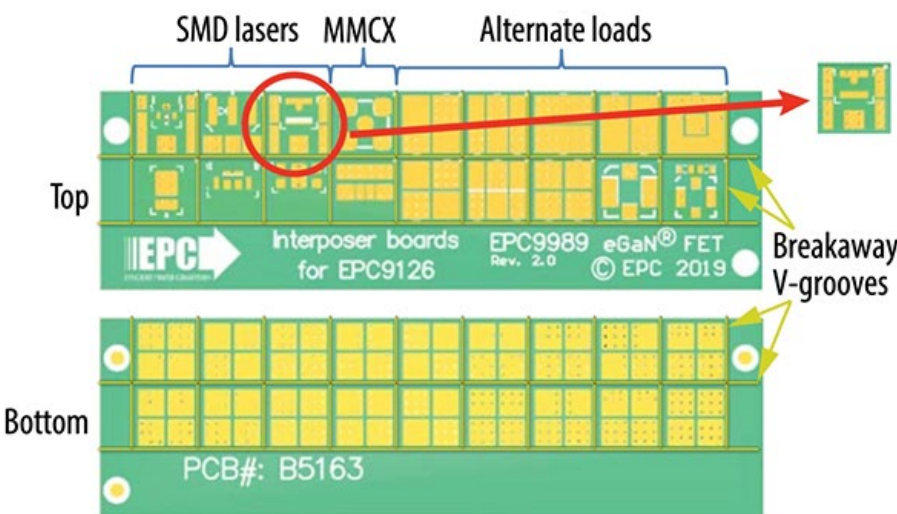
Figure 5: The EPC9989 interposer board provides a collection of interposers, such as the SMD laser interposer shown at the top right, that can be snapped off for use with the EPC9179 demo board. (Image source: EPC)
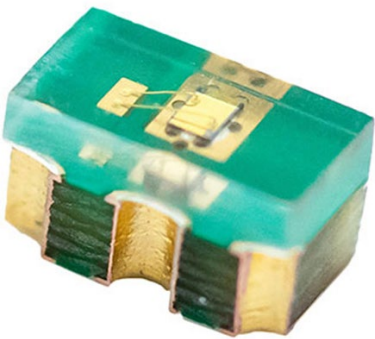

Figure 6: The TPGAD1S09H pulsed laser produces very high peak pulses and can emit light parallel or perpendicular to the mounting plane. (Image source: Excelitas)

The development board comes with an EPC9989 interposer board comprising break-away 5 x 5 mm interposers (Figure 5). These correspond to the mounting footprints of many common surface-mount laser diodes, such as SMD and MMCX, as well as the patterns designed to accommodate RF connectors and a wide variety of other loads.

Excelitas Technologies' TPGAD1S09H pulsed laser (Figure 6), emitting at 905 nanometers (nm), can be used with the EPC9989 interposer board. This laser diode uses a multi-layer monolithic chip mounted on a leadless laminate carrier to provide excellent thermal performance with a wavelength temperature coefficient (Δλ/ΔT) of 0.25 nm/°C. This quantum-well laser supports rise and fall times of <1 ns with an appropriate driver. The TPGAD1S09H can be used in surface-mount applications and hybrid integration. It can emit light parallel or perpendicular to the mounting plane, and the epoxy resin encapsulation supports low-cost and high-volume manufacturing.

The SPL S1L90A_3 A01 from ams OSRAM (Figure 7) is another example of a laser diode that can be used with the EPC9989 interposer board. This single-channel 908 nm laser module can deliver pulses ranging from 1 to 100 ns with a peak output power of 120 watts. It supports an operating temperature range of -40 to +105°C with a duty cycle of 0.2% and comes in a compact QFN package measuring 2.0 x 2.3 x 0.69 mm.

For LiDAR systems that require extremely narrow pulse widths, designers can turn to Texas Instruments' LMG1025-Q1, which is a single-channel, low-side gate driver with a 1.25 ns output pulse width capability that enables powerful LiDAR systems meeting IEC 60825-1 Class 1 safety requirements. Its narrow pulse width capability, fast switching, and 300 picoseconds (ps) pulse distortion enable precise LiDAR ToF measurements over a long range.
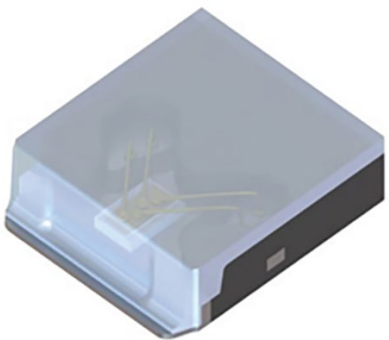

Figure 7: The SPL S1L90A_3 A01 laser diode produces pulses ranging from 1 to 100 ns and can be used with the EPC9989 interposer board. (Image source: ams OSRAM)

A propagation delay of 2.9 ns improves the control loop response time, and the 2 x 2 mm QFN package minimizes parasitic inductance, supporting high-current, low-ringing switching in high-frequency LiDAR drive circuits. The LMG1025-Q1EVM is an evaluation module for the LMG1025-Q1 that has a place to accommodate a resistive load to represent a typical laser diode, or for mounting a laser diode after drive pulse tuning with a resistive load (Figure 8).
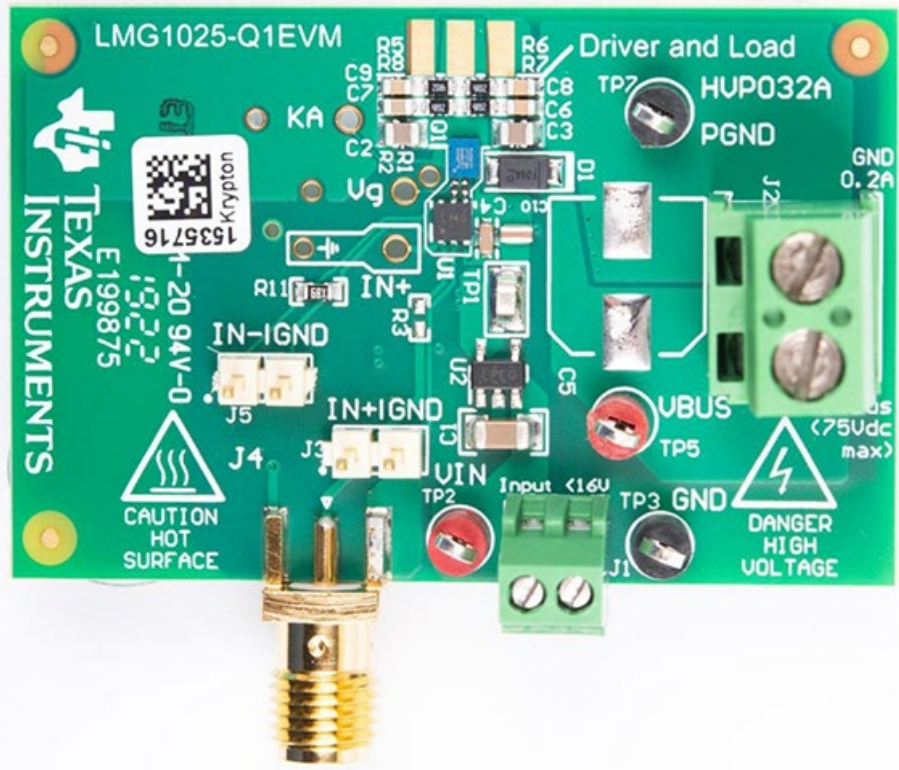
Figure 8: The LMG1025-Q1EVM demo board can accommodate a resistive load representing a typical laser diode for initial setup. (Image source: Texas Instruments)

Conclusion

Designers are increasingly challenged to develop automotive LiDAR systems that deliver real-time ToF measurements with centimeter resolution that meet the Class 1 safety requirements of IEC 60825-1. As shown, GaN FETs can be used with a variety of laser diodes to produce the nanosecond pulse widths and high peak-power levels needed in high-performance automotive LiDAR.

Recommended reading

Ensure LiDAR Automotive Distance Sensor Precision with the Right TIA

Get Started Quickly with 3D Time-of-Flight Applications

Frank J Sprague and the Richmond Union Passenger Railway

By David Ray
Cyber City Circuits

FIRST TROLLEY CAR SYSTEM IN RICHMOND

In 1888, the world's first successful electric railway, the Richmond Union Passenger Railway, branched at this point to link downtown and Jackson Ward with the suburbs. This system, designed by Frank Julian Sprague (1857-1934), contained 12 miles of track with 40 trolley cars running to Byrd Park in the West End and to 29th and Broad streets in the East End. This model system that revolutionized urban transportation ceased operation in November, 1949.

DEPARTMENT OF CONSERVATION AND HISTORIC RESOURCES. 1985

1830s-1880s – The problem with public mass transportation

There was a time before the luxury of quick and easy transportation for the masses existed.

Transportation was a problem during the mid-nineteenth century. The Second Industrial Revolution was spinning up and the world was quickly becoming industrialized. New manufacturers were emerging, but they needed human labor to operate them. People started leaving their farms to come to the urban centers. Factories and mills were being built faster than the houses and roads needed to support them.

Inside the city, business and invention would meet over and over again, trying to solve the issue of mass public transportation. One very early example of a solution is the world's first subway, the 'London Underground' sometimes known as 'The Tube'.

Some cities also had 'street railroad' systems where a carriage would ride rails, pulled by horses or donkeys, carrying people and goods where they needed to go. According to the census, by 1880, there were over two thousand miles of horsedrawn 'street railroads' in America. [1] Multiple times a day, a team of people had to keep the tracks maintained and clean the animal waste off the rails.

Eventually, some towns had steam trains that ran a circuit around different areas of their city, allowing people to travel. However, these trains left the areas they drove through covered in smoke and filth. Because of this, most cities forbade steam streetcars in their business and central districts, so they were mainly used in the outer area of a metropolis. [2]

Some places, like San Francisco, California, started using 'cable streetcars'. In this system, a large cable would span the entire length of the railway and it would pull or drag the streetcar along the track. While these were very efficient and clean, the high initial investment made most cities continue to use animal power.

Quickly, the convenience of the 'street railroad' became a nuisance caused by the pollution.

Werner von Siemens' Electromote

The dawn of the electric streetcar

Toward the end of the nineteenth century, gas-powered trains and streetcars started appearing, but they would bring many of the same problems as their steam-powered counterparts. The electric streetcar was the solution to many of the problems created by steam and animal-drawn streetcars, but it also brought about its own set of challenges and limitations.

In 1882, Werner von Siemens developed the first electric trolly streetcar, *Elektromote*. Essentially an experiment and novelty, the Elektromote operated on a track a third of a mile long for less than two months, from April 29 to June 13, 1882. Following this innovation,
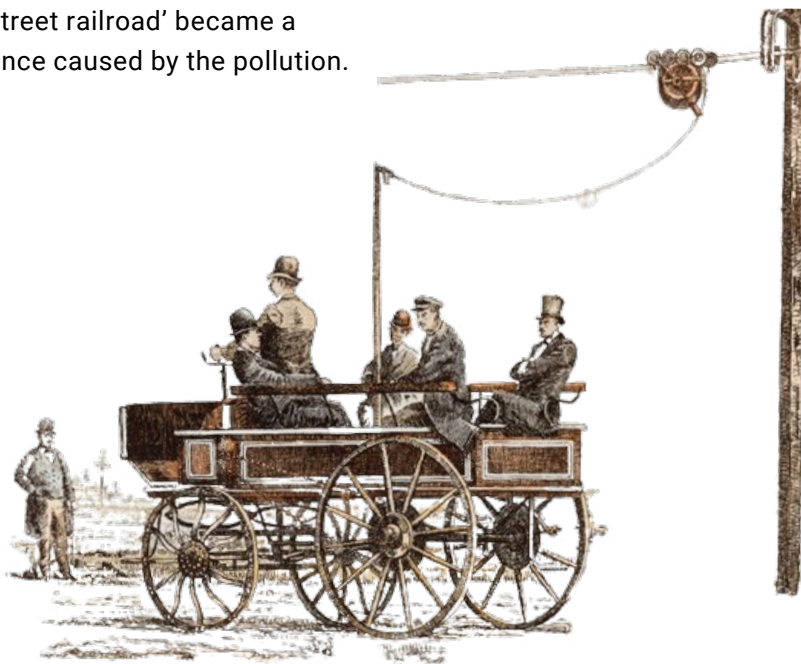
Successful Electric Street Railway.

RICHMOND, VA., Oct. 28.—The new electric line of the Richmond Union Passenger Railway Company, running entirely through this city, is about finished and the first car was run over it last night. The success was complete. This line covers a distance of twelve miles—the longest electric road in the world. People here are jubilant over the result of the trial trip.

Osgood Ripley Journal | Osgood, Indiana s | Nov 3, 1887

many worked tirelessly over the next several years to produce and market a practical electric streetcar system. By 1888, there were only thirteen electric streetcar systems in America and less than fifty miles of 'electric street railroad' were installed nationwide. [2]

The opening of the Richmond Union Passenger Railway in 1888 marked a leap in mass transit technology. While there were dozens of attempts before this, it's opening had the most impact on the industry overall. The first large-scale electric streetcar system officially introduced electric vehicles to the masses. The success of this system in Richmond, Virginia, spurred the adoption of electric streetcars in cities all over America.

The electric streetcar allowed cities to grow and become larger centers of industry.

The inventor: Frank J Sprague

Frank J Sprague was born in Milford, Connecticut, on July 25, 1857. At age 9, his mother, Francis Sprague, died from tuberculosis, and soon after, his father, David Sprague, abandoned his children with Frank's aunt, Ann Sprague [3].

At an early age, Frank excelled academically. He was fascinated by mechanical devices and electricity and spent much of his childhood building various contraptions, showcasing a talent for engineering.

Following High School, his community raised the money needed for him to take an exam in Springfield, Massachusetts, for the US Army's West Point Academy. However, when he arrived, he found that he had arrived at the testing for the US Naval Academy at Annapolis. Perhaps not bothered by this, he took the exam and joined the Navy as an officer candidate at Annapolis, where he studied mechanics and electricity. [3]

After finishing his classes at Annapolis, he was assigned to the USS Richmond as a midshipman. Sprague's time on the Richmond is an important part of his journey as an engineer and inventor. While serving on the Richmond in the Philippines from May 1879 to February 1880, Sprague kept a

detailed notebook with 169 pages filled with his inventions and ideas. [3] This period was critical in honing his skills and creativity, laying the groundwork for his future contributions to electrical engineering.

Sprague's notebook included sketches and descriptions of various devices, such as an 'electric light,' 'duplex telephone,' 'quadruplex and octoplex telegraph systems,' a motor, and a means of transmitting facsimiles of pictures by wire. His meticulous documentation of these inventions demonstrates his passion and drive to innovate.

Sometime in 1880, Sprague got orders back to Annapolis for examinations, after which he was commissioned as an Ensign. Not long after, he found himself on the USS Lancaster in Europe.

A visit to London, England

It was January 1882 when the young Navy ensign took leave in London to visit the Crystal Palace Electrical Exposition. While in London, Ensign Frank J Sprague rode on the world's first subway. The 'Metropolitan Railway' was established in 1863 as an underground train system using coal-powered steam-driven engines.

The cars were crowded with hundreds or thousands of people, and the air was full of smoke. The walls of the tunnels were filthy and covered in soot.

There are historical cases where people have reported illness after using the Metropolitan Railway, including 'The Case of Elizabeth Stainsby' who died soon after traveling in the London Underground. This was one of the only underground subway systems in the world, and imagine that being your first experience.
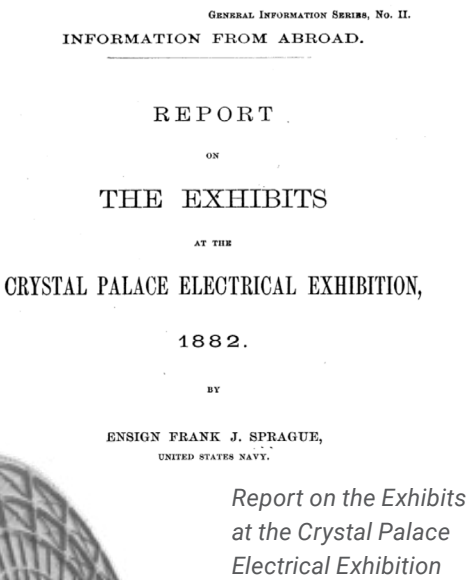

Cadet Frank Sprague

1882 - The Crystal Palace Exposition

The Crystal Palace Electrical Exposition in London was the largest of its kind. Young Sprague quickly advocated for making himself a judge at the event. He was placed on the judging panel for gas engines, dynamo-electric generators, and electric lamps, where he first met Edward H. Johnson and Thomas Edison.

While aboard the USS Lancaster in France, Frank J Sprague wrote a report about the Crystal Palace Electrical Exposition for the Secretary of the Navy. In this report, he recounts many things he saw as a judge and an observer." Historians tend to agree that this experience in London shaped the path of his innovation. Without orders on the USS Lancaster, one can wonder if the history of electric transportation would be the same.

"Frank Sprague also attended the 1876 Centennial Exhibition, where Alexander Graham Bell unveiled his invention 'The Telephone'."

General Information Series, No. II.

INFORMATION FROM ABROAD.

REPORT

ON

THE EXHIBITS

AT THE

CRYSTAL PALACE ELECTRICAL EXHIBITION,

1882.

BY

ENSIGN FRANK J. SPRAGUE,
UNITED STATES NAVY.

Report on the Exhibits at the Crystal Palace Electrical Exhibition

The Crystal Palace of Hyde Park, London

A new era for transportation

1883 – Working for Edison

While at the 1882 Crystal Palace Electrical Exhibition, he impressed Thomas Edison and his business partner Edward H. Johnson. So much so that when he resigned his commission with the Navy, he readily found a position at Edison's Menlo Park in New Jersey.

He was placed on the team building power transmission lines in towns and cities. While there, he developed new techniques for building transmission lines. Soon, he found that he could build anything he had in mind. He found a local machine shop and started prototyping the designs that had been stored in his notebooks for many years.

While working on this, he came to the realization that he could never rise to the level of Thomas Edison's glory and wealth while he was working for him. He saw the fame and wealth that came along with being a genius inventor and businessman, and he wanted it.

Around this time, in May 1883, he filed for his first patent for the Electro-Dynamic Motor. This motor was novel in that it could keep a constant speed, no matter the load. This was key because a streetcar needs to be predictable and controllable, whether one passenger or twenty, and at the time they were not.

Sprague wanted to be a heroic and famous inventor who got the newspaper's front page, but he knew he could never do that in Edison's shadow.
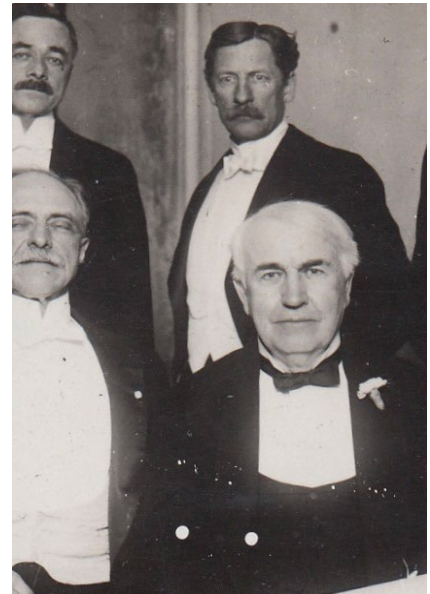
Sprague stands behind Thomas Edison, Philadelphia 1915

1884 – Sprague Electric Railway and Motor Company

In March of the following year, 1884, Sprague was awarded patent number 295,454. With the patent, unusual confidence, and unreasonable determination, the 27-year-old man left a promising career working for the 'Wizard of Menlo Park' to strike out on his own. From 1884 to 1890, Sprague Electric Railway and Motor Company, sometimes called SERM, focused on building a full-scale electric railway system.

While developing his designs and ideas, he worked with other streetcar companies performing repairs and retrofits. This gave him plenty of opportunities to learn the industry quickly, whereas Edison would have kept him engineering power transmission lines.

Up to 1888, there had been no less than seventy-four attempts to create a practical electric railway system. [4] Even Edison attempted an electric streetcar with a mile-long track and a car that could go forty miles an hour [3]. The field of 'electric traction' was growing at a rapid pace.
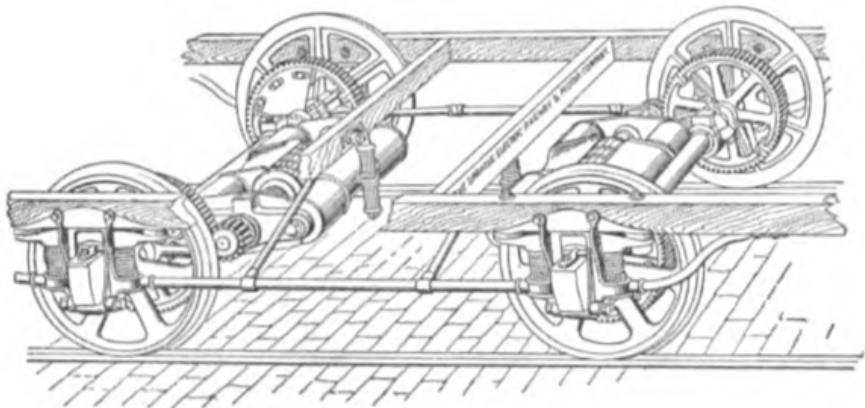
To this point, most electric systems of the day were only meant to replace the horses with an engine in order to continue using the streetcars that horses once pulled. Sprague was poised to revolutionize the industry with his 'under-running trolley' idea.

1888 - Richmond Union Passenger Railway

Working with investors and other engineers, the Sprague Electric Railway & Motor Company gained a contract to build an electric streetcar system in Richmond, Virginia. This was noteworthy because of the area's topology. There are reports of the earlier animal-pulled streetcars being called 'horse-killers' because of the steep inclines.


Earliest type of Sprague motors used in Richmond.

Other electric streetcars couldn't manage the hilly terrain and steep inclines, while Sprague's unique design for independent direct drive of each streetcar could. Each streetcar had its own motors underneath the passenger cab.

From August 1887 to February 1888, Sprague, with his engineers and laborers, built the Richmond

Union Passenger Railway. When it first opened, the track was twelve miles long and had forty cars, making it the longest electric railway in the world. Each of the forty cars could run independently and navigate the ten-degree inclines through the city.

The Richmond Union Passenger Railway included many new innovations. Two of the most pivotal were the 'trolley pole' and the 'trolley wheel'. Before this, electric streetcars would use electrified rails or an overhead wire to carry current. The trolley pole differed in that it would run underneath the overhead wire, making each car easy to remove from the line at any point by simply pulling down the trolley pole. The electric power was produced by a local generation plant, powered by coal and steam.

Sprague's unique undercarriage motors made the steep inclines a trivial task.
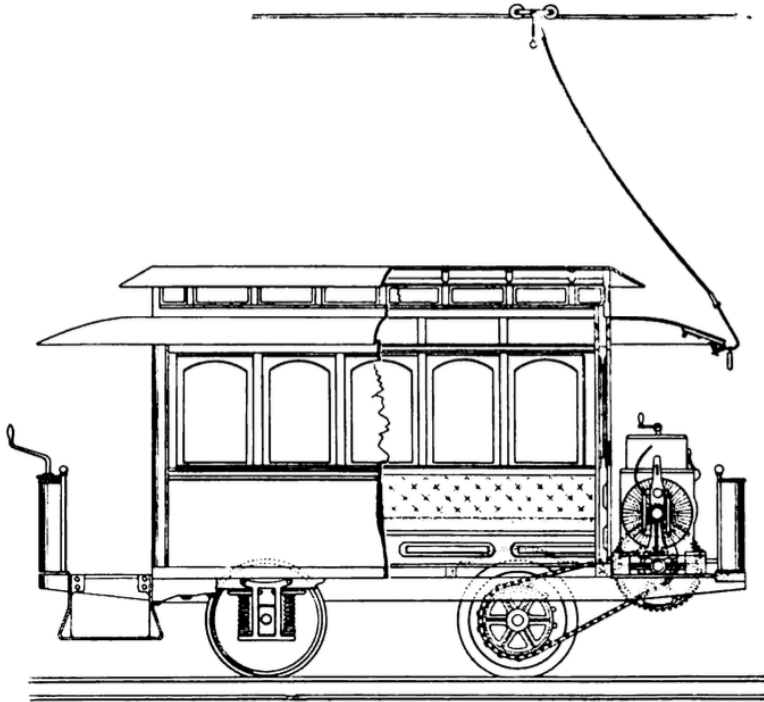
Example of a competitor's streetcar by Van Depoele.

Other streetcars of the time would have the motor on the front, with a heavy chain connecting the motor to the axle. Sprague's design placed the motor underneath the streetcar, connecting it directly to the wheels, delivering more torque and horsepower than any competitor could with a similarly sized motor.

All of this came together the Summer of 1888 when the Richmond Union Passenger Railway opened and became the 'first successful electric railway' in history. It would continue to operate from 1888 to 1949.
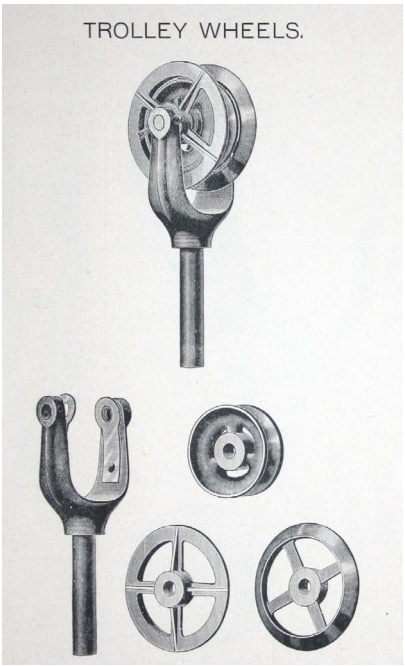
Catalog page from the age selling parts for streetcars.

West End Railway of Boston

Soon after the opening, Sprague met with the head of the 'West End Railroad' of Boston, who wanted to install cable cars (like the ones used in San Francisco) in Boston, being skeptical that an electric streetcar could work in a high traffic environment. Sprague rigged the system to prove that his system could operate dozens of cars simultaneously. He instructed the engineers to load slugs in the fuses and increase the generator's power to five hundred volts. [5]

Then, with the wave of a lantern, he had twenty-two streetcars on the far end of a line designed for only four streetcars moving along one after another. In his book 'The Growth of Electric Railways', he says when they started, the lights all went dim, and the voltage dropped to two hundred volts, but soon all of the cars overcame their initial inertia, and they were soon merrily running along.

This test was conclusive, and the fate of the cable in Boston was Settled. From this point, to 1890, some reports say that Sprague had purchase orders for upto two hundred streetcar systems throughout the county.

Beyond streetcars: Sprague's broader impact on technology

In 1890, Sprague Electric Railway and Motor was absorbed by Edison General Electric. It was here when the real problems with Edison started, with Edison removing Sprague's name and replacing it with the word EDISON. The irony is that he left Edison's company six years earlier to avoid this exact thing from happening. Sprague's wife, Harriet Sprague, writes about this experience in her book 'Frank J Sprague and the Edison Myth,' some years after his death.

After feeling bamboozled by Edison, he decided to leave the streetcar business altogether—for a while anyway. He would continue changing the world by developing the first practical electric elevator, regenerative braking, and electric locomotives. In 1906, he was responsible for electrifying New York's Grand Central Terminal lines.

Many consider Frank J. Sprague to be one of the most influential inventors of the nineteenth and early twentieth centuries. Unfortunately,

his legacy has been shadowed by Thomas Edison, but many of his inventions and techniques are still used today in freight trains and elevators worldwide.

Sprague raised a family that returned to North Adams, where his son Robert C. Sprague started Sprague Electric Company. Sprague Electric became renowned for its innovation in electronic components, particularly tantalum capacitors. In the 1960s, his son, John L. Sprague, became more involved and directed the company towards the new world of semiconductors, where it was successful for many years.

Suggested reading

Engineering Invention: Frank J. Sprague and the U.S. Electrical Industry by Frederick Dalzell

The Mechanization of Urban Transit in the United States by Eric Schatzberg

Report on The Exhibits at the Crystal Palace Electrical Exhibition by Frank J. Sprague

American Experience: The Race Underground

Frank J Sprague and the Edison Myth by Harriet Sprague

Frank J Sprague: Seventy-Fifth Anniversary

Richmond Union Passenger Railway IEEE Milestone Listing

The Growth of Electric Railways by Frank J Sprague

Sprague Legacy: Electrical Inventions and Innovation

References

[1] "Report on Transportation Business in the United States at the Eleventh Census," U.S Government Printing Office, Washington, DC, 1894.

[2] E. Schatzberg, "The Mechanization of Urban Transit in the United States," in Technological Cpmpetiveness (Ed: William Aspray), IEEE Press, 1993.

[3] F. Dalzell, Engineering Invention: Frank J. Sprague and the U.S. Electrical Industry, Cambridge, Ma: The MIT Press, 2010.

[4] "IEEE Milestones: Richmond Union Passenger Railway, 1888," [Online]. Available: https://ethw.org/Milestones:Richmond_Union_Passenger_Railway,_1888. [Accessed 2024 07 21].

[5] F. J. Sprague, The Growth of Electric Railways, Atlantic City, NJ: American Electric Railway Association, 1916.

Timeline

July 25, 1857
Frank J Sprague is born in Milford Connecticut

1866
Mother dies and he moves to North Adams, Massachusetts

1874
Sprague starts attending the Naval Academy in Annapolis, Maryland.

1876
The Centennial Exposition in Philadelphia

1878 - 1880
Sprague leaves Annapolis and is assigned to the USS Richmond.

1881 - 1883
Serves on the USS Lancaster in Europe

1882
Served on the Jury at the 1882 Crystal Palace Exposition in London

1883
Left the Navy to Work for Edison

May 1883
Files First Patent Application – Dynamo-Electric Motor
  • Patent Link

1884
Leaves Edison to Start the Sprague Electric Railway & Motor Company

1886
Invents Regenerative Braking

1888
Opens the Richmond Union Passenger Railway (Twelve Miles in Length with Forty Cars)

1890
Contracts 200 Trolley Systems

1890
Sells to Edison General Electric

How to use residual current monitors to ensure electrical safety when charging electric vehicles

By Jens Wallmann
Contributed By DigiKey's European Editors

Frequent charging of the high-voltage battery of electric vehicles (EVs) translates to high mechanical stress requirements for charging cables and connectors. If the insulation breaks and live metal parts are exposed, or shunts appear in the onboard electronics, life-threatening residual currents can occur in the EV user's body. Particularly problematic are various DC residual current forms that cannot be detected by the AC-sensitive Type-A residual current devices (RCDs).

To prevent electric shock accidents, manufacturers of EV supply equipment (EVSE) must incorporate RCDs into their power electronics products that trip within a few milliseconds for both AC and DC residual currents of a few milliamperes (mA).

This article explains forms of residual currents, how to measure them, and where to install the RCD in the charging circuit. It then introduces residual current monitors (RCMs) from Littelfuse that system designers can use to add protection against DC electric shock in their EVSE devices in a cost and time-efficient manner. The article also demonstrates which EV charging modes these current sensors are suitable for and how they are used.

Residual currents in the EV charging circuit

Charging EVs at voltages up to 400 volts AC and 1000 volts DC requires extensive protective measures for the EV user when handling charging equipment. Due to the harmonic-rich and asymmetric switching pulses of charging stations and onboard chargers, as well as several hundred volts of DC link voltage, various types of AC and DC residual currents can occur via shunts, coupling effects, insulation faults, and leakage faults.

Power electronic circuits such as rectifiers, switching converters, frequency inverters, along with inverter and phase-angle control systems, have a wide variety of load current characteristics. The resulting potential residual currents are categorized as sinusoidal AC, pulsed DC, and straight DC. These residual current forms are dangerous to humans. Table 1 shows typical load current signals of various circuit topologies and the resulting residual current waveforms. Columns 1 to 3 assign RCD types suitable for detection.

Table 1: Fault current forms and their detection according to the type of RCD that is most suitable (columns 1 to 3). (Image source: Wikipedia)

27

we get technical

Tripping characteristic of RCD types

In general, personal protection against electric shock on electrical installations is regulated by IEC 60479 and UL 943. Both standards define significant AC and DC residual currents in the range of 6, 30, 100, 300, 500, and 1000 mA, at tripping times ranging from 20 to 500 ms. Common tripping thresholds in the EV charging circuit are 6 mA DC and 30 mA AC.
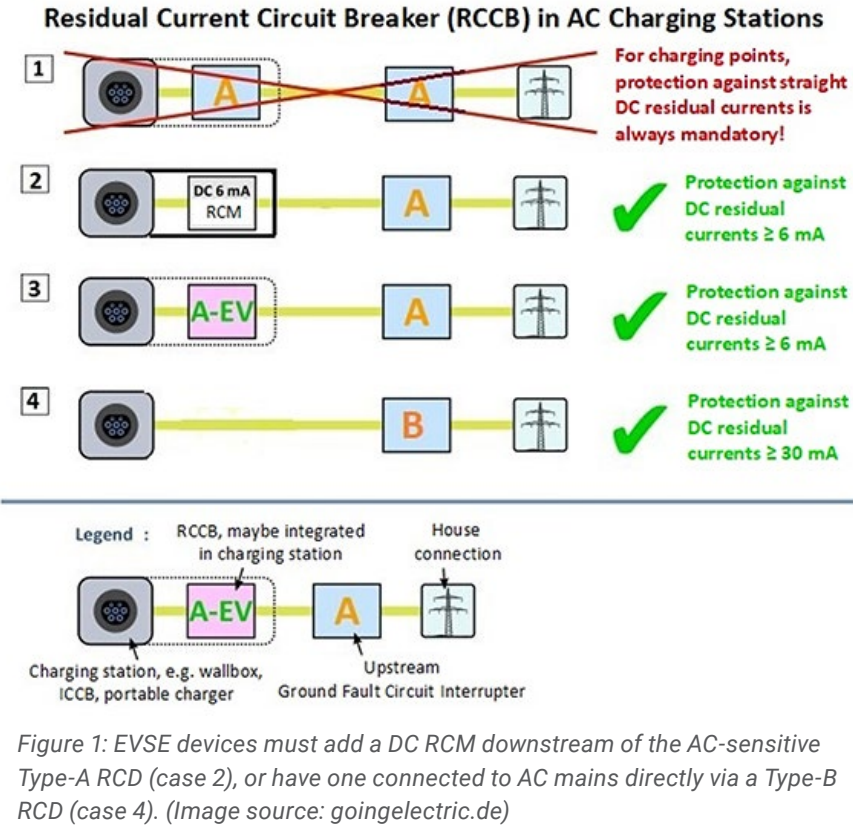
System designers can now easily implement specific personal protection requirements in the charging circuit by selecting an RCD type of the appropriate standard. Table 2 lists residual current forms and trip tolerance of the different RCD or ground fault circuit interrupter (GFCI) types.

Installing RCDs in the EV charging circuit

Type-A or Type-F RCDs only detect AC residual current and DC pulsating current, which is insufficient for protecting an EV charging circuit. A wide range of straight DC residual currents that can occur in the onboard charger or battery management system must also be considered.

Type of residual current	Form of residual current	Permissible tripping current range	GFCI or RCD Type				
			Type AC	Type A	Type F	Type B	Type B+
Sinusoidal AC	∿	0.5 … 1 I$_{\Delta n}$	●	●	●	●	●
Pulsating DC (positive or negative half-waves)	⌒⌒	0.35 … 1.4 I$_{\Delta n}$	–	●	●	●	●
Phase angle controlled half-wave currents (positive or negative half-waves)			–	●	●	●	●
Phase angle of 90° electrical		0.25 … 1.4 I$_{\Delta n}$					
Phase angle of 135° electrical		0.11 … 1.4 I$_{\Delta n}$					
Pulsating DC superimposed with straight DC of 6 mA		max. 1.4 I$_{\Delta n}$ + 6 mA	–	●	●	●	●
Pulsating DC superimposed with straight DC of 10 mA		max. 1.4 I$_{\Delta n}$ + 10 mA	–	–	●	●	●
Mixed frequency current generated by single-phase frequency converters		0.5 … 1.4 I$_{\Delta n}$	–	–	●	●	●
Straight DC		0.5 … 2 I$_{\Delta n}$	–	–	–	●	●
High and mixed frequency current generated by three-phase frequency converters			–	–	–	●	●
Frequency 150 Hz		0.5 … 2.4 I$_{\Delta n}$					
Frequency 400 Hz		0.5 … 6 I$_{\Delta n}$					
Frequency 1,000 Hz		0.5 … 14 I$_{\Delta n}$					

Table 2: Tripping characteristics of different GFCI or RCD types. (Table source: abb.com)

Figure 1: EVSE devices must add a DC RCM downstream of the AC-sensitive Type-A RCD (case 2), or have one connected to AC mains directly via a Type-B RCD (case 4). (Image source: goingelectric.de)

Figure 2: Illustration of the four charging modes defined in the IEC 61851 standard. (Image source: bestchargers.eu)

The IEC 62196 standard, therefore, defines two residual current protection options: the use of an all-current sensitive RCD of Type B (or Type B+), or an RCD of Type A in conjunction with a residual DC monitoring system according to IEC 62955 with IΔn DC ≥ 6 mA. The DC fault current monitoring can be arranged in the wall box, in the building electrical installation, or at both locations.

Since an AC-sensitive Type-A or Type-F RCD is usually present in building electrical systems, designers can cost-effectively add 6 mA residual DC monitoring to Mode 3 wall boxes or charging stations, as well as to the in-cable control boxes (ICCB) of Mode 2 charging cables (Figure 1, cases 2 and 3).

Charging modes for EVs

The EV battery can be charged via different charging modes, depending on the available on-site power connection, connection plug, charging cable, and the charging technology installed in the vehicle, as well as in the charging station. In Europe, the electrical energy can be fed into the vehicle via single-phase AC (230 volt/3.6 kilowatt (kW), three-phase AC (400 volts/22 kW), or via high-voltage DC charging stations (up to 1000 volts DC/500 kW). Figure 2 illustrates the four charging modes defined in the IEC 61851 standard.
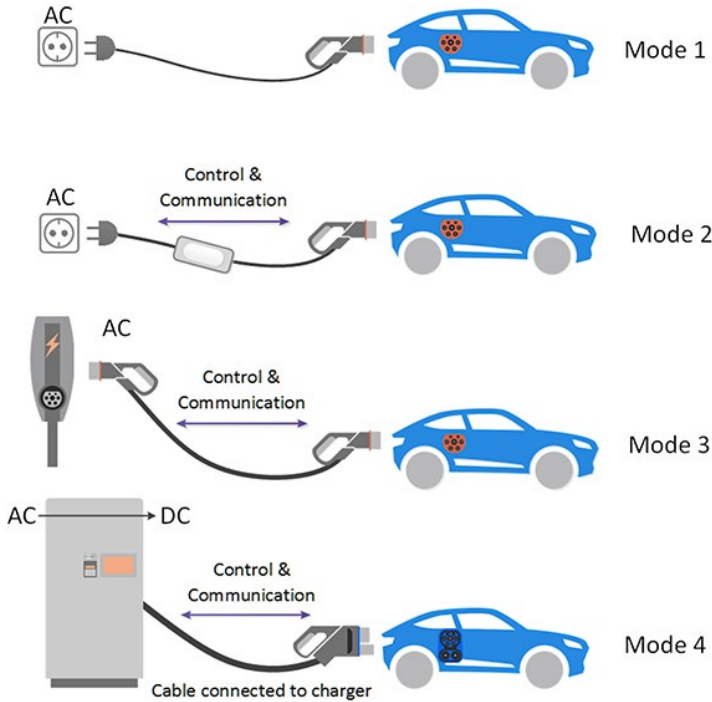
Mode 1 *(single-phase AC charging up to 3.6 kW; default mode of charging)*

In this case, the electric or hybrid vehicle is connected to a standard 230-volt household socket using a simple passive cable and will be charged using low power at a maximum of 3.6 kW via the onboard charger. This charging scenario does not provide sufficient protection against residual DC for the user. Usually, only an AC-sensitive Type-A RCD is installed in the building's electrical system.

Mode 2 *(single/three-phase AC charging up to 22 kW via an ICCB charging cable)*

A Mode 2 charging cable equipped with a Type 2 vehicle plug contains an ICCB that performs safety and communication functions when charging EVs using domestic and three-phase sockets to prevent overloading them.

The following protection functions must be integrated with the ICCB:

- Determination of polarity and protective conductor (PC) monitoring; only a few ohms of loop impedance are permitted between neutral and the PC.

- Testing of the electrical connection between the PC and the metal body.
- An AC and DC residual current circuit breaker prevents current accidents.
- Monitoring/shutdown of the charging process in the event of anomalies (for example, current fluctuations due to corroded plug contacts or cable breakage).
- Monitoring of the temperature inside the ICCB and both plugs and perform shutdown if necessary.

- Control of the charging power: Pull-down resistors on the control pilot (CP) wire to signal the cable current load rating to both the wall box and the EV; the pulse width modulation (PWM) signal on the charging control (CC) wire signals the wall box charging power capability to the EV.

Mode 3 *(single-phase/three-phase AC charging up to 22 kW via wall box)*

For EV charging, a passive Mode 3 cable is connected to a wall box in private households or a public AC charging station in parking lots. Both have integrated the same protection functions as the ICCB above.

Mode 4 *(direct battery DC fast charging up to 500 kW)*

DC high-power charger (DC/HPC) stations for EVs deliver significantly higher charging currents compared to Mode 2 and Mode 3. Shock protection from residual AC and DC is implemented in this supercharger; the different charging cables are always firmly attached.

Measure AC and DC fault currents in the EVSE circuit

RCMs, from the RCM14 series from Littelfuse Inc., detect DC and/or AC residual currents in AC or DC systems and deliver an
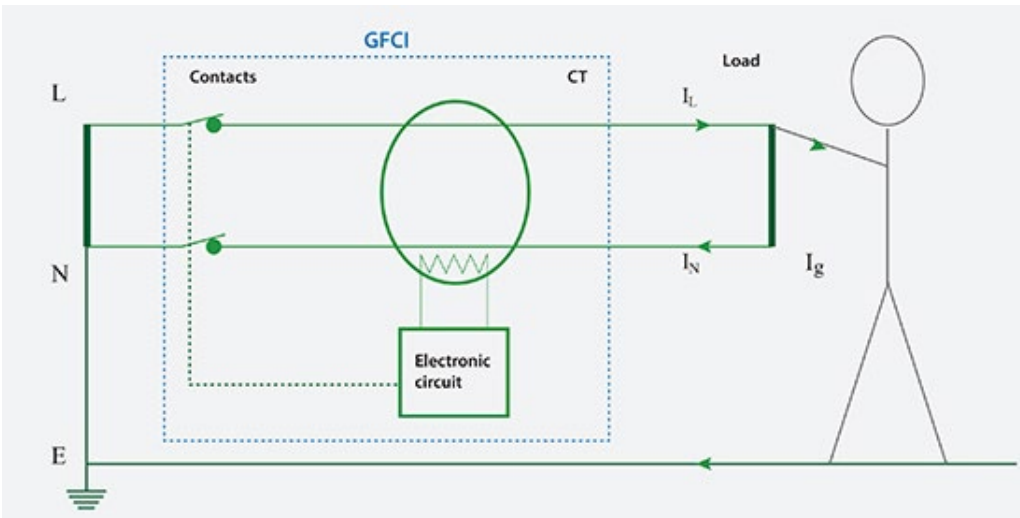

Figure 3: If a fault current (I_g) flows into the ground potential via the human body, the GFCI total current differs from zero, and the circuit breaker trips. (Image source: Littelfuse)

output signal to control an external disconnect (cutoff relay). In contrast, RCDs and residual current circuit breakers (RCCBs) have an integrated cutoff relay.

AC residual currents are detected using an inductive current transformer (CT). For this purpose, the current forward conductor (IL) and current return conductor (IN) are fed through a soft magnetic toroidal core, causing both current vectors to normally compensate for each other and add up to zero. If a fault current (I_g) flows into the ground potential via the human body in the circuit behind the detector, the RCM or GFCI total current differs from zero, and the circuit breaker trips (Figure 3).

By integrating a fluxgate magnetometer probe into a slot of the toroidal core and compensating the magnetic flux to zero by means of a compensation coil, the CT can also detect differential DC. More accurate than Hall effect sensors or shunt resistors, this method detects tiny DC fault currents from 6 mA at heavy DC load currents up to 500 amperes (A).

RCMs featuring control output for disconnector

Littelfuse's RCM14 series is ideal for use in ICCB charging cables for EVs (Mode 2) and EV charging stations (Mode 3). They are available in three residual current detection options in accordance

with IEC 62752 (Mode 2), IEC 62955 (Mode 3), and UL 2231.

Each RCM has one operation LED and one fault LED. The four-pin JST connector simplifies the installation: pins 1 and 2 are for the 12-volt power supply, pin 3 is for external function testing, and pin 4 is an open-drain switching output to drive an external disconnector such as a cutoff relay, at up to 100 mA and 24 volts (maximum) (Figure 4).

Figure 4: The RCM14 series modules have two status LEDs and are easy to connect via the four-pin JST connector. (Image source: Littelfuse)

These active RCMs can also be used to detect AC and/or DC residual currents in single-phase or multi-phase DC installations. Single-phase operation limits the load current to 100 A, while three-phase operation is at 40 A. They can handle load current pulses up to 3000 A.
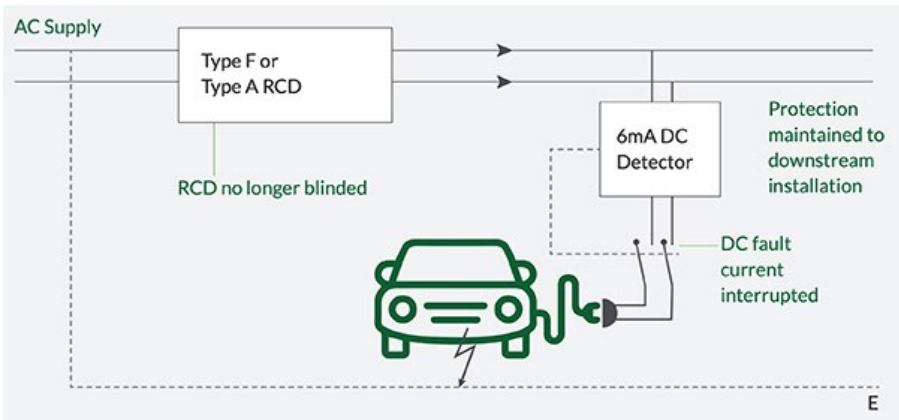

Figure 5: RCM14-01 adds monitoring of DC residual currents ≥ 6 mA to AC-sensitive Type-A RCDs in building electrical systems. (Image source: Littelfuse, Western Automation)

RCM14-01: 6 mA DC RCM module according to IEC 62955, 14 millimeter (mm) aperture

The RCM14-01 residual current monitor detects DC fault currents in 50 Hz/60 Hz AC systems. It is developed for use in Mode 3 charging stations for EVs (IEC 62955 standard) to interrupt the charging circuit of the EV in the event of a DC fault current ≥ 6 mA. This detector adds DC residual current monitoring function to existing Type-A and Type-F RCDs of the building's electrical system in a cost-effective and simple manner (Figure 5).

RCM14-03: 6 mA DC/30 mA AC RCM module according to IEC 62752, 14 mm aperture

The RCM14-03 is intended for use in ICCB or integrated protection devices for EVs in charging Mode 2

to interrupt the supply to the EV in the event of an AC or DC fault.

RCM14-04: 56 mA DC/20 mA AC RCM module according to UL 2231-2, 14 mm aperture

The RCM14-04 module detects AC and DC fault currents in 60 hertz (Hz) AC installations. It is designed for use in Charging Circuit Interrupting Device (CCID) EV charging station applications where it interrupts the supply to the EV in the event of an AC and/or DC residual current condition.

RCM20-01: The RCM20-01 is a residual current monitor intended for the detection of DC residual currents in 50 Hz/60 Hz AC installations. It is intended for Mode 3 Electric Vehicle Charging Stations, to disconnect the supply to the Electric Vehicle under DC residual fault current condition.

The product is fully compliant with IEC 62955.

RCM20-03: The RCM20-03 is a residual current monitor intended for the detection of DC and AC residual currents in 50 Hz/60 Hz AC installations. It is intended for Mode 2 Electric Vehicle Charging Stations, to disconnect the supply to the Electric Vehicle under DC and AC fault current condition. The product is fully compliant with IEC 62752, and can also be used for IEC 62955 applications where 30 mA AC fault detection is required.

For integration in a larger device circuit, the following RCM modules presented are also available as open-frame systems:

- RCM14-01_SYS_V, RCM14-01_SYS_H
- RCM14-03_SYS_V, RCM14-03_SYS_H
- RCM14-04_SYS

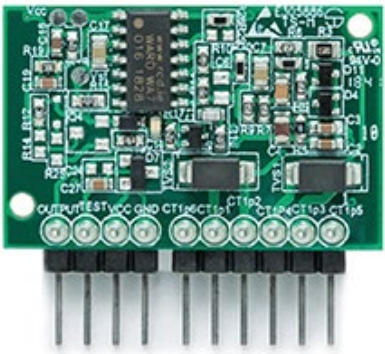Each system consists of a solderable sensor pc board and a separate current transformer (Figure 6).

Figure 6: The RCM14-04_SYS modules are open-frame systems consisting of a sensor pc board and a current transformer. (Image source: Littelfuse, Western Automation)

Conclusion

AC-sensitive Type-A RCDs are common installation standards in building electrical systems, but they cannot protect against DC residual current hazards in EV charging circuits. As shown, the RCM14 series can perform the DC residual current monitoring required in ICCB charging cables (Mode 2) and EV charging stations (Mode 3). Featuring only four connection pins, system designers can easily and cost-effectively implement the compact RCM module or the open-frame system in their EVSE.

The selection and use of FPGAs for automotive interfacing, security, and compute-intensive loads

By Clive "Max" Maxfield
Contributed By DigiKey's North American Editors

Traditionally, computation tasks in automobiles have been performed by microcontroller units (MCUs) and application processors (APs). A typical mid-range vehicle can contain 25 to 35 MCUs/APs, while luxury cars may employ 70 or more. Increasingly, automobiles require extremely sophisticated, computationally intensive capabilities for such tasks as advanced driver assistance systems (ADAS), infotainment, control, networking, and security. Many of these applications involve machine vision in the form of image and video processing coupled with artificial intelligence (AI).

Alone, the processor architecture struggles to handle all of the electrical interfaces and protocols that are demanded by peripheral devices like sensors, cameras, and displays. Also, in many cases, these processors simply cannot satisfy the extreme computational demands of tasks like machine vision and AI.

To address this complexity, designers of automotive systems are turning to field-programmable gate arrays (FPGAs), not to replace the existing MCUs/APs, but rather to act as bridges between them and other devices, and to augment them by offloading communications and other computationally intensive tasks.

Since FPGAs can be programmed to support a wide variety of electrical interfaces and protocols, they can act as bridges between MCUs/APs and sensors, cameras, and displays. Also, because they can perform calculations and operations in a massively parallel fashion, FPGAs can be used to execute computationally intensive vision processing and AI tasks, thereby freeing up the host processors for other activities.

This article discusses the processing requirements of modern vehicles and describes some of the automotive applications that can be addressed by FPGAs. It then introduces some example FPGAs from Lattice Semiconductor and shows how they can be used to solve connectivity, processing, and security problems. Associated development boards are also presented to help designers get started.

Target automotive applications for FPGAs

To support their ADAS capabilities, today's automobiles employ many sensors outside the vehicle, including cameras, radar, LiDAR, and ultrasonic detectors. In many cases, it is necessary to take data from disparate sensors, pre-process this data (removing noise and formatting it as required),

and use sensor fusion to combine the data such that the resulting information has less uncertainty than would be possible if the data from the different sensors were to be used individually. In many cases, AI applications are employed to analyze the data, make decisions, and take appropriate actions.

A relatively recent trend is the deployment of electronic (also known as "digital") rear-view mirrors. In this case, a wide-angle, high-resolution camera is installed inside the rear window.

The video stream from this camera is presented on a digital display that replaces the traditional mirror, resulting in a clear rearward view that is unobstructed by passengers in the rear seats. In some cases, video streams from cameras mounted on the side mirrors may be merged with the video stream from the rear window camera. These three feeds are "stitched together" to provide a single image that is presented on a super-wide electronic mirror, thereby providing the driver with a much higher degree of situational awareness as to what's going on around the vehicle.

Another recent trend is to deploy in-cabin cameras mounted on the dashboard, on the steering column, or integrated into the rear-view mirror (regular or electronic). When coupled with AI, these in-cabin mirrors can be employed for a wide variety of tasks, such as recognizing who is sitting in the driver's seat and adjusting it and the mirrors accordingly. In addition to monitoring drivers to ensure they're paying attention to the road and not dozing off, such a system can also look for signs of drowsiness, as well as medical problems or distress such as an epileptic fit or heart attack, and take appropriate actions. These actions may include activating the hazard warning lights, applying the brakes, and guiding the vehicle to the side of the road. Further applications include ensuring young children and pets are not mistakenly left unattended in the rear seats by preventing the car from being locked and flashing the lights, and alerting the driver if a passenger leaves something like a phone, bag, or package on the back seat.

With regard to video-based applications, in some cases, it is required to split a single video input into multiple streams; in others, a design requirement may be to aggregate multiple video streams into one.

With the increasing deployment of electric vehicles (EVs) comes the need to monitor and control motors, and to monitor and manage the charging process to achieve maximum battery life.

On top of all of this, many of today's automobiles are starting to be 5G or V2X enabled, where V2X ("vehicle to anything") refers to communication between a vehicle and any other entity that may affect (or be affected by) the vehicle, from roadside infrastructure to other vehicles. Along with this connectivity comes the need for security to prevent the vehicle from being hacked.

Automotive-grade devices

It's important to remember that not all FPGAs are suitable for automotive applications. The Automotive Electronics Council (AEC) is an organization originally established in the 1990s by Chrysler, Ford, and GM for the purpose of establishing common part qualification and quality system standards. One of the most commonly referenced AEC documents is AEC-Q100, "*Failure Mechanism Based Stress Test Qualification for Integrated Circuits*."

IATF 16949:2016 is a technical specification aimed at the development of a quality management system which provides for continual

improvement, emphasizing defect prevention and the reduction of variation and waste in the automotive industry supply chain and assembly process. Based on the ISO 9001 standard, IATF 16949:2016 was created by the International Automotive Task Force (IATF) and the Technical Committee of ISO.

Electronic system suppliers to the automotive market increasingly require that semiconductor suppliers provide products compliant to the AEC-Q100 standard, and can demonstrate ISO/TS-16949 certification of their quality systems.

Choosing the right FPGA for the job

FPGAs are extremely flexible, but different device families offer various combinations of capabilities and functions that make them better suited to specific tasks. In the case of embedded vision applications, for example, modern cameras and displays often employ MIPI interfaces. The MIPI CSI-2 (camera/sensor) and DSI (display) protocols both employ a communications physical layer (PHY) called the D-PHY. Legacy MCUs/APs may not support this interface, but some FPGAs do, such as CrossLink-NX embedded vision and processing FPGAs from Lattice Semiconductor.

In addition to two hardened four-lane MIPI D-PHY transceivers supporting 10 gigabits per second (Gbits/s) per PHY, CrossLink-NX devices also support 5 Gbits/s PCIe, 1.5 Gbits/s programmable inputs/outputs (I/O), and 1066 megabits per second (Mbits/s) DDR3. These devices also support traditional electrical interfaces and protocols like low-voltage differential signaling (LVDS), Sub-LVDS (a reduced-voltage version of LVDS), Open LVDS Display Interface (OLDI), and serial gigabit media-independent interface (SGMII). As a result, these devices can be used for aggregating video streams, splitting video streams, running AI applications, and—while doing all of this—also act as bridges between legacy MCUs/APs and modern sensors and displays.

Developers of automotive systems looking to evaluate CrossLink-NX FPGAs will find the combination of the LIFCL-VIP-SI-EVN CrossLink-NX VIP Sensor Input Board (Figure 1) and the LF-EVDK1-EVN Modular Embedded Vision Kit to be of interest (the former can act as an input board for the latter). In addition to a CrossLink-NX FPGA, the sensor input board also features four, 13 megapixel Sony IMX258 CMOS MIPI image sensors, supporting 4K2K @ 30 frames per second (fps) or 1080p @ 60 fps. It also supports easy sensor connectivity via three independent PMOD interfaces.
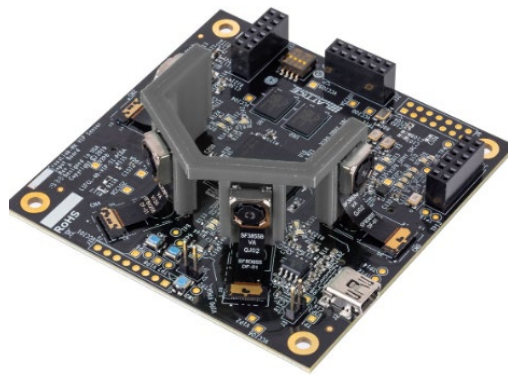
Figure 1: The CrossLink-NX VIP Sensor Input Board, which can act as input to the Embedded Vision Development Kit, contains a CrossLink-NX FPGA and supports the aggregation of four MIPI Sony IMX258 image sensors. (Image source: Lattice Semiconductor)

For compute-intensive applications that also demand high I/O bandwidth—such as AI for tasks like gesture recognition and control, voice recognition and control, human presence detection, occupant identification, and driver monitoring—Lattice's ECP5 FPGAs feature up to 3.2 Gbit/s serializer/deserializer (SERDES), up to four channels per device in dual-channel blocks for higher granularity, up to 85K look-up tables (LUTs), enhanced digital signal processing (DSP) blocks that provide 2x resource improvement for symmetrical filters, and single event upset (SEU) mitigation support. These FPGAs also provide programmable I/O support for LVCMOS 33/25/18/15/12, XGMII, LVTTL, LVDS, Bus-LVDS, 7:1 LVDS, LVPECL and MIPI D-PHY I/O interfaces.

An example ECP5 device is the [LFE5U-85F-6BG554C](#) with 84,000 logic elements, 3.75 megabits (Mbits) of RAM, and 259 I/Os. Also of interest is the [LFE5UM-45F-VERSA-EVNG](#) ECP5 Versa Development Kit (Figure 2). The board uses a half-length PCI Express (PCIe) form factor and allows designers to evaluate key connectivity features of the ECP5 FPGA, including PCIe, Gigabit Ethernet (GbE), DDR3, and generic SERDES performance.
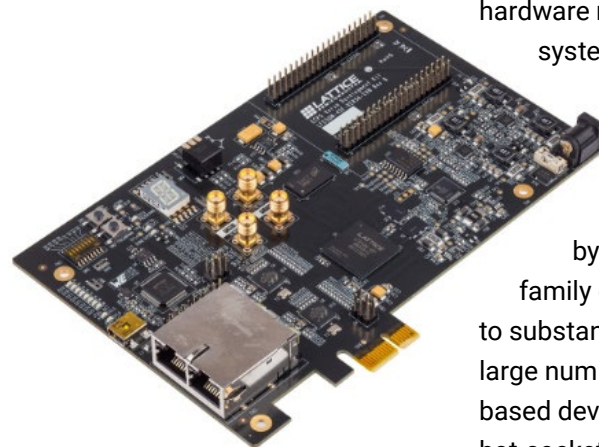

Figure 2: Presented in a half-length PCI Express form-factor, the ECPe Versa Development Kit lets designers evaluate key connectivity features of the ECP5 FPGA, including PCIe, GbE, DDR3, and generic SERDES performance. (Image source: Lattice Semiconductor)

Securing automobiles using FPGAs

Security threats from hacking are increasing, with new breaches constantly occurring. In the case of automobiles, a cyberattack could cause loss of control resulting in injury or death to the passengers and pedestrians, and damage to the car, other vehicles, and property.

A large part of an automobile's security solution is to establish a root of trust (RoT); that is, a hardware resource within the system that can always be trusted. One solution is an FPGA-based hardware RoT (HRoT), such as that provided by Lattice's MachXO3D family of devices. In addition to substantial LUT resources and large numbers of I/O, these flash-based devices offer instant-on and hot-socketing capabilities. General-purpose applications include glue logic, bus bridging, bus interfacing, motor control, power-up control, and other control logic applications.

Of particular interest is the fact that the MachXO3D is the only FPGA with both dual-boot capability and less than 10K LUTs that is equipped with a hard National Institute of Standards and Technology (NIST)-certified Immutable Security Engine. This allows the MachXO3D to act as the automobile's HRoT in the form of the system's first-on,

last-off device. When the system is powered up, the MachXO3D first checks to make sure that it's running authenticated firmware. It then checks the firmware of the other devices in the system. If any of the components in the system are attacked or compromised, including itself, the MachXO3D rejects the suspect firmware and reloads that component with a known-good, authenticated firmware image.

For those developers interested in evaluating MachXO3D-based designs, the [LCMXO3D-9400HC-D-EVN](#) MachXO3D Development Board provides an extensible prototyping platform (Figure 3). The board features an L-ASC10 (analog sense and control) hardware management device, a general-purpose I/O interface for use with Arduino and Raspberry Pi boards, two Hirose FX12-40 header positions (DNI), an Aardvark header (DNI), and 128 Mbit serial peripheral interface (SPI) Flash with quad read feature.

The board comes in a 4 x 6-inch form factor and features a USB mini-B connector for power and programming, and multiple header positions supporting Arduino, Aardvark, FX12, Hirose and Raspberry Pi. Both a USB cable and a quick start guide are included.

Figure 3: The MachXO3D Development Board features a MachXO3D FPGA, an L-ASC10 (analog sense and control) hardware management device, support for Arduino and Raspberry Pi boards, two Hirose FX12-40 header positions (DNI), an Aardvark header, and a USB-B connection for device programming. (Image source: Lattice Semiconductor)

Conclusion

Modern automotive electronics require an ever-increasing number of sensors, electrical interfaces, and protocols, with corresponding demands on processing power and bandwidth. The addition of AI and machine vision processing, as well as security requirements, complicate the implementation of solutions using classic MCU or AP approaches.

As shown, by appropriate application of FPGAs, designers can add a degree of flexibility and processing power that can bridge disparate processing environments, perform sensor aggregation and fusion functions, address I/O bandwidth requirements, and perform calculations and operations in a massively parallel fashion, while freeing up the host processors for other activities.

For security, a flash-based FPGA with dual-boot capability and NIST-certified Immutable Security Engine can act as the automobile's HRoT and ensure that it—and other devices—are running only authenticated firmware, thereby preventing hackers from cryptographically compromising the automobile's systems.

Further reading

[Fundamentals of FPGAs: What Are FPGAs and Why Are They Needed?](#)

AEC-Q200 qualified fuses play a critical role in the automotive environment

By Rolf Horn
Contributed By DigiKey's
European Editors

Fuses have been used as essential protective devices since the dawn of electrical lighting in the late nineteenth century. They protect devices from faults such as short-circuits occurring at a load by interrupting the flow of electric current. This interruption can protect wiring, electronic devices, and the load from catastrophic damage. Therefore, fuses can minimize the fault condition risk of injuries to people and property.

The protection fuses provide is especially beneficial to the growing automotive market and the rising demand for electric vehicles (EVs). With EV power conversion and the ever-increasing number of electronic systems, circuit protection has become an imperative to safeguard the myriad of devices present in an EV.

Automotive fuses

The typical automotive fuse works by melting a conductive link. An electric arc follows, turning the link into an open circuit. The current pulse (magnitude, shape, and time), the ambient temperature, and the characteristics of the fuse determine the temperature within the fuse element at which this occurs. The time-current curve (called TCC) at different rated fuse currents helps determine the interrupt time at a given current. This, along with the melting energy (I^2 x t, where I is the current and t is the time), helps determine a suitable fuse for the application. Automotive fuses have evolved to meet the changing needs of the industry. In the 1960s, glass tube fuses were commonly used. More compact blade fuses are the most used today. Most of these are fast responding (in a few milliseconds), which is good to prevent damage to sensitive electronics, but not for motors due to the high inrush current at start-up. Slow blow fuses have been developed for this application, where the response time can be in the order of several seconds. Some of the other characteristic requirements for fuses used in automotive applications include:

- Higher voltages of up to 800 V for the changing bus are expected soon. For this reason, ratings exceeding 1,000 V will be required, with great attention given to the arc discharge created at these voltages to prevent circuit damage.

- High reliability due to the risk of catastrophic accidents due to failure.

- Large range of ambient temperature. Fuses used in the engine compartment can face temperatures ranging from -40˚C to +150˚C or wider.

- Size, weight, and form factor are key minimization goals for all components used in an EV, driven by the need to increase vehicle performance and range for a given battery charge.

- Vibration resistance is a key requirement due to varied road conditions and driving profiles.

The AEC-Q200 automotive standard

Chrysler, Ford, and General Motors established the Automotive Electronics Council (AEC) in the 1990's to create a common quality system and unify part qualification standards for automotive applications. The AEC-Q200 standard covers the stress test qualification for passive components. The earlier Rev D of AEC-Q200, which has been active since June 2010, covered components such as resistors, capacitors, transformers, resonators, crystals, resettable fuses, thermistors, and varistors. This standard covered two main stress categories for the passive components:

- Environmental stress: This includes temperature cycling, humidity bias, high temperature storage, and high temperature operating life tests.

- Physical stress: This includes vibration, mechanical shock, solderability and resistance to soldering heat, flammability, terminal strength, and resistance to solvents.
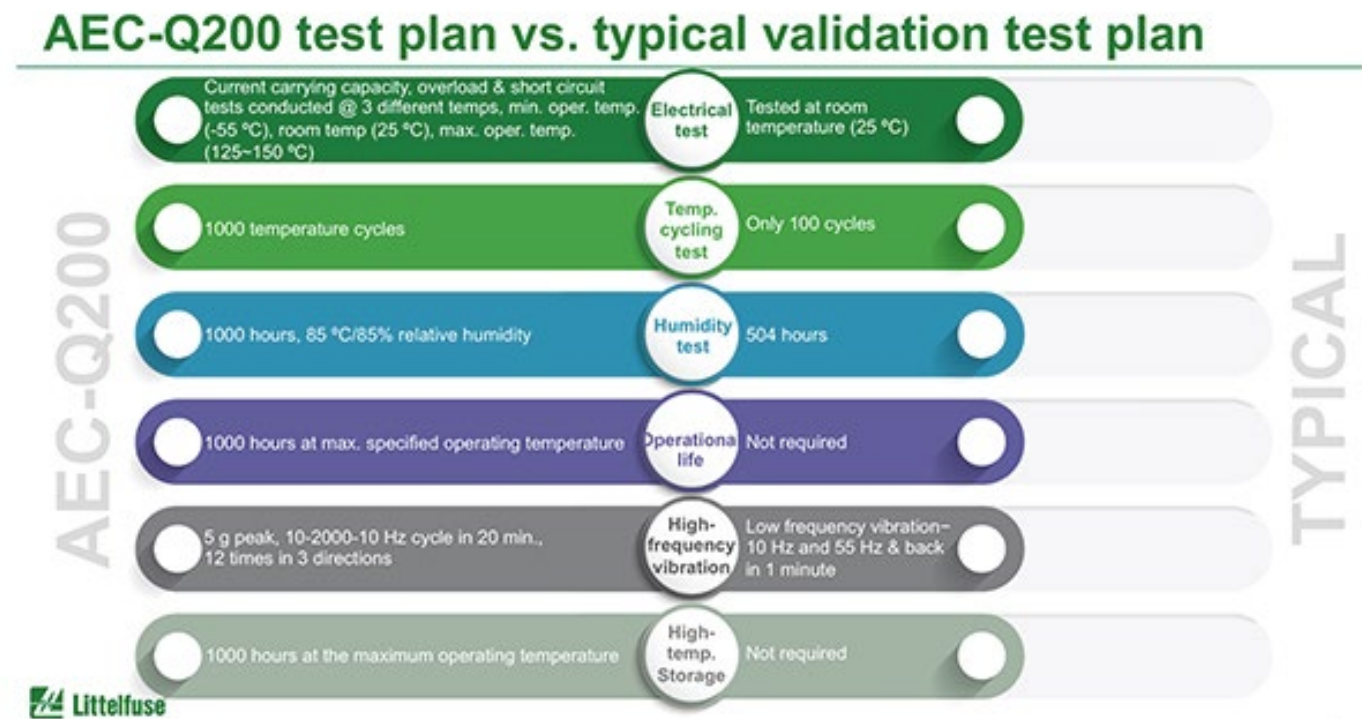
Figure 1: A representation of the AEC-Q200 Rev E stress tests specified for fuses. (Image source: Littelfuse)

The Rev E update to AEC-Q200, released in March 2023, adds the reliability requirements for fuses. As shown in Figure 1, Rev E includes a comprehensive list of stress tests that encompass both the environmental and physical stress factors mentioned above.

As shown in Figure 1, the AEC-Q200 Rev E stress conditions are stricter than typical non-automotive tests. Some key tests are now added, such as the operational 1,000 hours life test at the maximum specified operating temperature. The test methodology for fuses requires

pre-stress and post-stress resistance measurements, along with current carrying capacity and overload tests done post-stress. The goal of AEC-Q200 Rev E is to provide a common standard that manufacturers can use to design and test fuses used in the automotive market.

Littelfuse AEC-Q200 Rev E qualified fuses

Littelfuse has a long history in automotive fuse development and production. They first introduced automotive fuses in the 1930s,

and their ATO® fast-acting blade fuses are considered the global standard. Littelfuse contributed to the development of the Rev E qualification stress tests for fuses, as their internal qualification tests for automotive fuses were already aligned with AEC-Q200 Rev E.

Below is a list of details on some of their AEC-Q200 qualified fuses:

- The cartridge 828 series features a high voltage rating of 1,000 V_{DC}, with an interrupt rating of 10 kA at the rated voltage. They are targeted for OBC and PDU.

- The surface-mount 885 Nano2® series has a voltage rating of up to 500 V_{DC}, with an available interrupt rating of 1,500 A at 350 V_{DC}. These compact fuses can be used in Li-ion battery packs, the BMS and HV DC/DC converters.

- The surface-mount thin film chip fuse series 437A features voltage ratings from 32 V_{DC} to 125 V_{DC} and an interrupt rating of 50 A at the rated voltage. With their small footprint and fast response time, these are

ideally suited for secondary circuit protection of compact automotive electronics such as the LED headlights, the navigations system, the TFT display, etc.

- The through-hole ceramic body PICOII® 521 series is a very fast acting fuse in a space saving sub-miniature package. The voltage rating is 75 V, with an interrupt current rating of 300 A at the rated voltage. These can be used for BMS protection.

Conclusion

EVs require more electronic and electrical power conversion components and modules. Fuses play a critical safety role, not just for the electronic components, wiring, and devices they protect, but also for the personnel operating the vehicle. The inclusion of fuses in the AEC-Q200 qualification standards ensures that these vital components meet a uniform standard. Littelfuse has a range of AEC-Q200-qualified fuses that can be used in a variety of EV overcurrent protection applications.
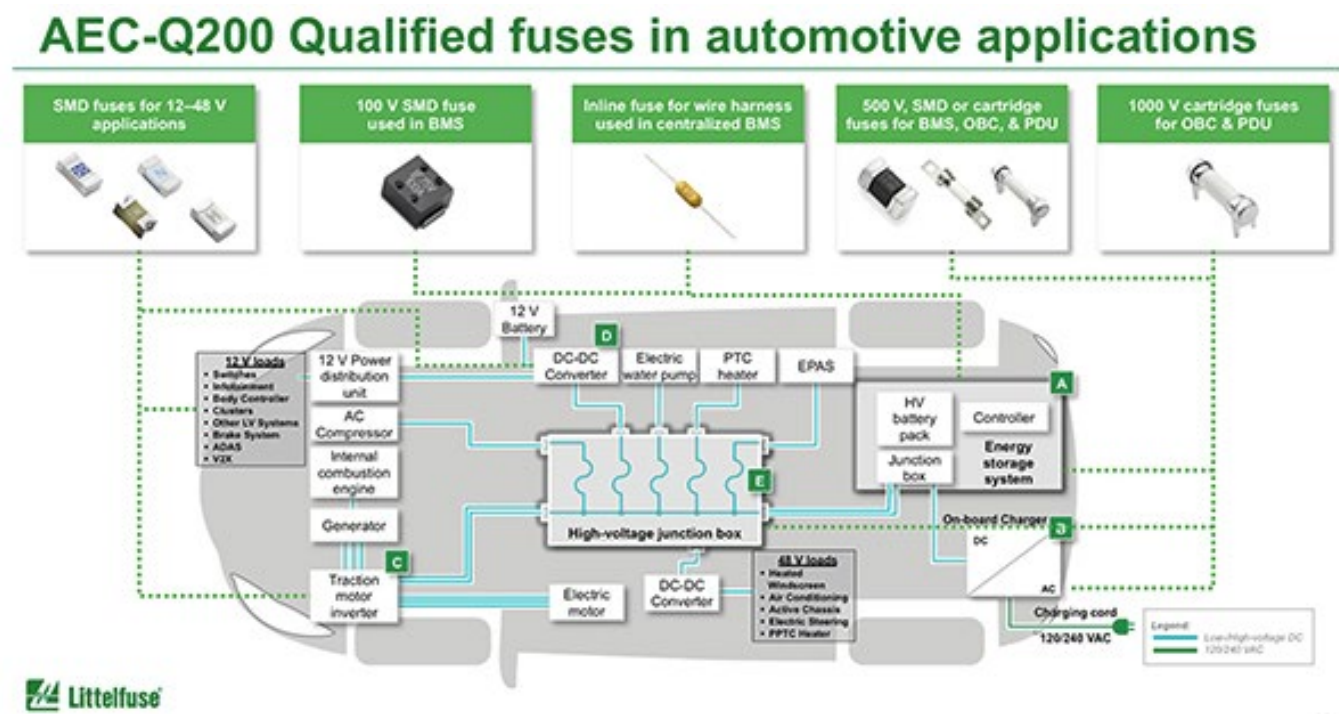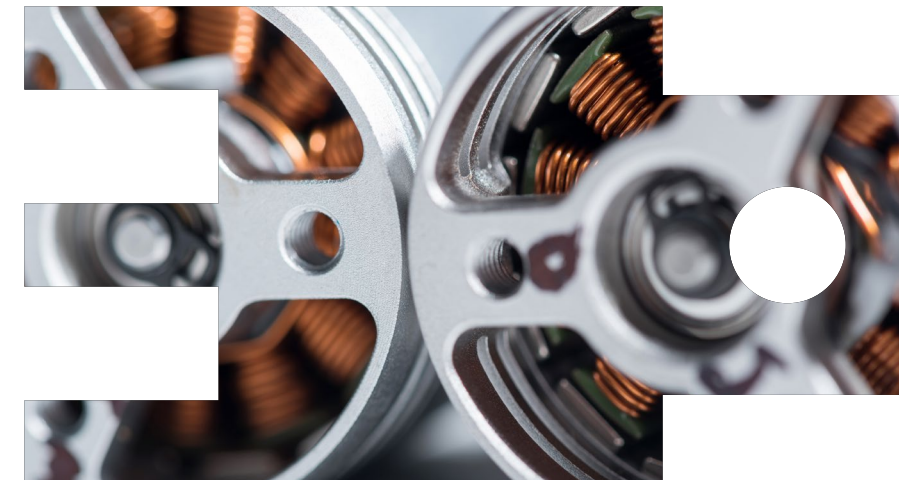

Figure 1: A representation of the AEC-Q200 Rev E stress tests specified for fuses. (Image source: Littelfuse)

Reduce EV range anxiety and improve safety using integrated FOC motor control and advanced sensors

By Jeff Shepard
Contributed By DigiKey's North American Editors

Designers of electric vehicle (EV) and hybrid electric vehicle (HEV) (often referred to as xEV) systems are under constant pressure to deliver more miles per charge to reduce range anxiety and lower vehicle carbon footprints. At the same time, they need to add more motors, sensors, associated electronics, processors, and software to meet higher levels of vehicle autonomy, user features, and safety, while also driving down costs.

Motors for doors, windows, battery cooling fans, radiator fans and pumps, and other features are a particularly thorny issue as not only do they add weight, they also require advanced control algorithms such as field-oriented control (FOC) to minimize noise and power consumption, while ensuring a smooth response. The overall system design task is complicated by the need to also meet ISO 26262 functional safety requirements and AEC-Q100 quality standards.

To meet these challenges, designers can turn to a variety of automotive qualified devices that provide higher levels of hardware and software that simplify the design and integration of various functions, while also reducing parts counts and overall footprint.

This article discusses the issues facing designers of EVs and HEVs. It then introduces and shows how to use a highly integrated FOC brushless direct current (BLDC) motor controller and an associated evaluation board to kickstart an efficient EV/HEV motor design. It also presents various sensors to monitor current, 3D position, speed, and direction, all from a single source, [Allegro MicroSystems](#).

The cost, safety, and range anxiety issues facing EVs

The issues that designers of xEVs must address are many, including vehicle cost, safety and reliability—particularly so in light of the increasing levels of vehicle autonomy, driving range per charge (range anxiety), and battery pack lifetime.

To support safety and reliability, advanced sensors are needed that meet the requirements of advanced driver assistance systems (ADAS) functions as defined in ISO 26262. For cost and range, designers have turned to higher voltage power rails of up to 800 volts for greater efficiency and reduced cable weight, while also taking advantage of improvements in battery pack design.

For example, better battery thermal management has contributed to greater driving range and longer battery life, while improved cooling for EV and HEV traction inverters helps to increase power and energy densities and reduce weight.

While higher levels of semiconductor device integration are enabling greater functionality with less weight and space, the BLDC motors required for the requisite cooling fans must be

tightly controlled to optimize efficiency. To achieve this, it's useful to include advanced motor-control algorithms such as FOC on the motor controller gate driver.

High-performance cooling

FOC enables smooth operation of electric motors over their entire speed range, and it can generate full torque at startup. In addition, FOC can deliver fast and smooth motor acceleration and deceleration, a feature that is useful for accurate control in high-performance motion applications. FOC can be used to develop high efficiency, compact and quiet low-voltage (LV) (50 volts DC and lower) drivers for a range of high-

performance BLDC motors up to 500 watts. These are typically used in xEV high-voltage (HV) battery cooling fans, as well as heating ventilation and air conditioning (HVAC) blowers, and liquid pumps for HV traction inverter cooling systems (Figure 1).

In conventional designs, FOC is implemented with external sensors using a microcontroller. Called direct FOC, these designs can be complex, and they tend to suffer from reduced dynamic response due to their reliance on external sensors to measure the motor's operating parameters.

FOC with improved performance and lower cost is possible by eliminating the external sensors.

The information from the missing sensors is still needed to implement FOC and can be extracted from the voltages and currents at the motor terminals from the back electromotive force (BEMF) in the motor windings. While the hardware is simpler, the implementation of sensorless FOC requires more complex control software.

A sensorless FOC algorithm can enable the highest efficiency and dynamic response while minimizing acoustic noise. It also provides a robust open-loop startup for when the motor is at a standstill when there is no BEMF information available.
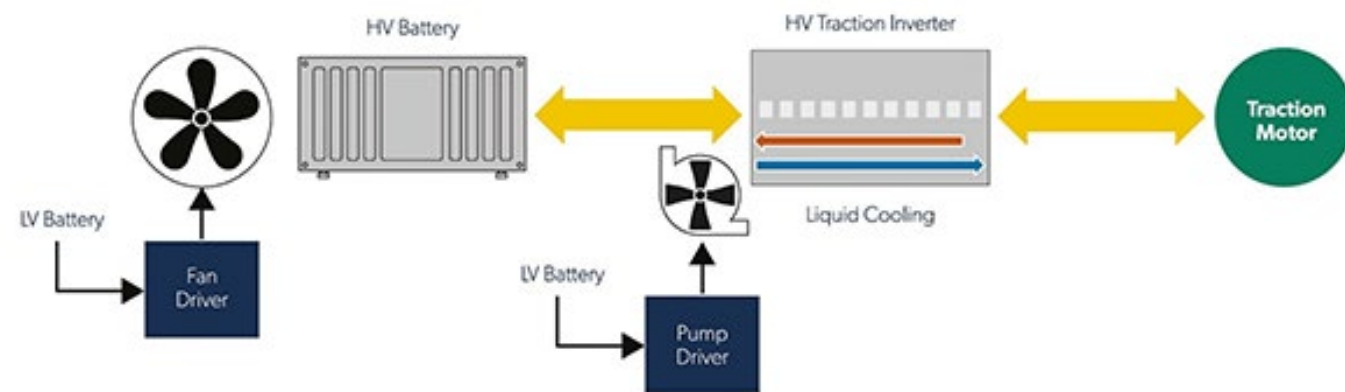
Easy FOC for automotive cooling fans and pumps

While most FOC BLDC drivers require software developers to write and port the algorithm to a microprocessor or microcontroller, the A89307KETSR-J from Allegro MicroSystems integrates the sensorless FOC algorithm directly into the gate driver. With only five external passive components (four capacitors and one resistor), the

A89307KETSR-J also minimizes the bill of materials (BOM), improves reliability, and reduces design complexity (Figure 2).

The A89307KETSR-J gate driver operates from 5.5 to 50 volts DC. The integrated FOC algorithm includes constant torque and constant power, as well as open-loop and constant speed operating modes. The A89307KETSR-J includes inputs

for pulse width modulation (PWM) or clock mode speed control, braking, and direction, and output signals for fault conditions and motor speed (Figure 3).

The A89307KETSR-J is optimized to drive external low-on-resistance N-channel power MOSFETs. It can supply the large peak drive currents needed to quickly turn the MOSFETs "on" and "off" in order to minimize power dissipation during switching, improving operating efficiency and reducing thermal management concerns. Multiple gate drive levels are available, enabling designers to optimize the tradeoff between electromagnetic interference (EMI) emissions and efficiency. Fast turn on of the MOSFETs reduces switching losses, but increases EMI, while slower MOSFET turn on reduces EMI, with the tradeoff being increased switching losses and lower efficiency.

Figure 2: A typical A89307KETSR-J xEV battery pack cooling fan application circuit shows the five external components: four capacitors and one resistor. (Image source: Allegro MicroSystems)
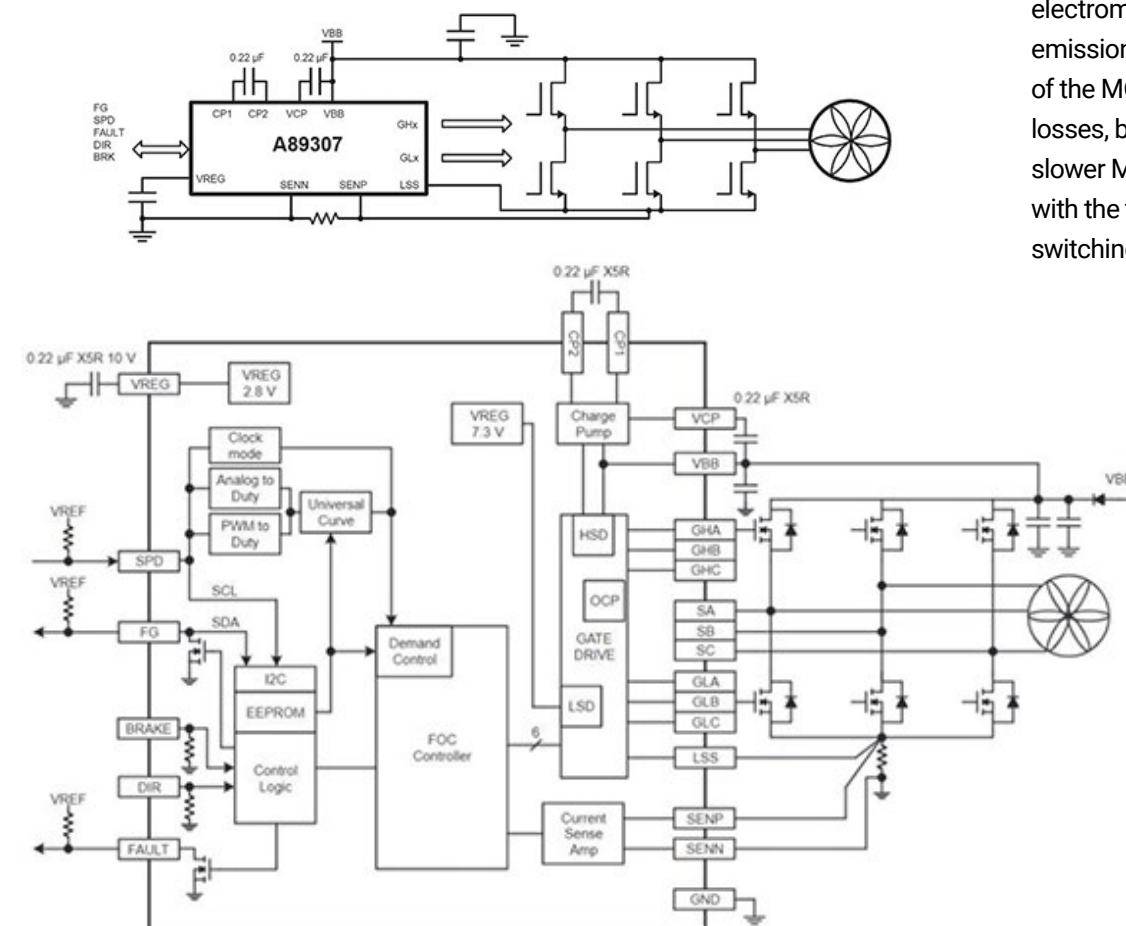

Figure 3: The A89307KETSR-J's internal block diagram shows the FOC controller (center), the PWM or clock mode speed control (SPD), brake (BRAKE) and direction (DIR) inputs (on the left), and the fault (FAULT) and motor speed (FG) outputs (also on the left). (Image: Allegro MicroSystems)

Figure 1: FOC motor controllers can use LV battery power to cool xEV HV batteries and HV traction inverters. (Image source: Allegro MicroSystems)

Motor speed can be controlled through PWM, analog, or CLOCK input. Closed-loop speed control is an option, with a programmable revolution per minute (RPM)-to-clock frequency ratio. The sensorless start-up control includes forward and reverse pre-rotation (windmill) detection and synchronization, enabling the A89307KETSR-J to operate over a wide range of motor and load configurations.
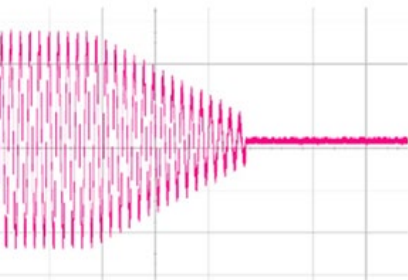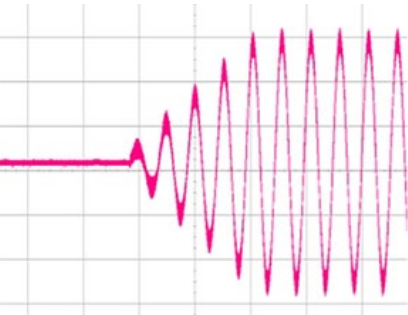
Allegro MicroSystems' Non-Reverse Startup algorithm also improves startup performance. The motor will start in the correct direction after power-up without reverse vibration or shaking. The Soft-On-Soft-Off feature gradually increases the current to the motor with the "on" command (windmill condition), and gradually reduces the current from the motor with the "off" command, further reducing the acoustic noise (Figure 4).

The A89307KETSR-J includes an I2C interface for setting the motor rated current, voltage, speed, resistance, and start-up profile. The I2C also implements on/off and speed control, as well as speed feedback and fault signals.

Sensorless FOC eval board

Designers can use the [APEK89307KET-01-T-DK](#) eval board and [associated software](#) to speed the development of FOC-based BLDC motor drives using the A89307KETSR-J (Figure 5). This board includes the A89307KETSR-J with access to all input and output pins plus a complete three-phase power stage for driving a BLDC motor. Designers can select FOC drive parameters using a simple graphical user interface (GUI) and load them into the on-chip EEPROM. The minimum BOM needs of the A89307KETSR-J enables the design of drives that fit inside the motor housing, further reducing solution size.

Figure 4: The A89307KETSR-J current waveforms for soft "on" (top) and soft "off" (bottom) result in smooth motor operation and reduced acoustic noise. (Image source: Allegro MicroSystems)

Figure 5: The APEK89307KET-01-T-DK eval board has the A89307KETSR-J (U1, center left hand side of the board) and six power MOSFETs (right hand side) to drive a BLDC motor. (Image source: Allegro MicroSystems)
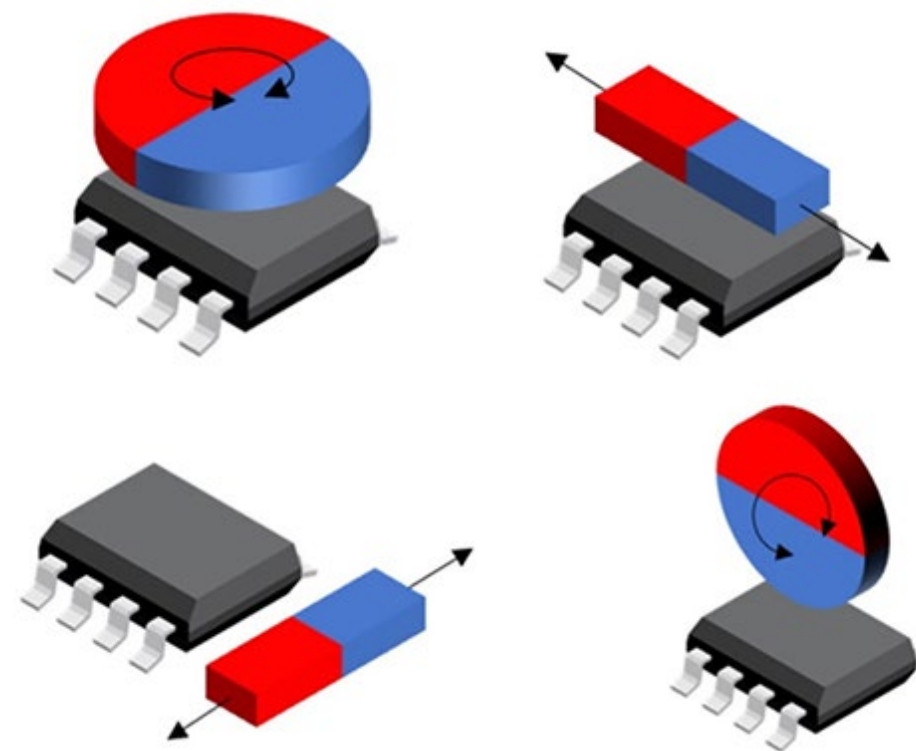

Figure 6: The A31315LOLATR-XY-S-SE-10 3D position sensor can measure rotary motion in the horizontal and vertical planes, and measure linear motion side to side or front to back. (Image source: Allegro MicroSystems)

Sensors for ADAS

Designers of xEV systems need to sense current levels in motor drives, DC-DC converters, and inverters, as well as the rotary positions of throttle valves and cylinders, and the speed and direction of the gears in transmissions to implement compact and cost-effective ADAS functions. Allegro MicroSystems offers a variety of sensor solutions for ADAS including:

Current sensing: The [ACS72981KLRATR-150B3](#) provides designers with economical and precise AC or DC current sensing. This high-precision

linear Hall-effect current sensor has a bandwidth of 250 kilohertz (kHz) and is designed for use in motor control, DC-DC converter control, inverter control, and load detection and management. It's an AEC-Q100 qualified IC and has a response time of <2 microseconds (µs), supporting the rapid overcurrent fault-detection needs of safety-critical applications.

3D position sensing: Contactless linear and rotary 3D magnetic position sensing for throttle, valve, cylinder, and transmission position detection can be quickly implemented using Allegro MicroSystems' [A31315LOLATR-](#)

[XY-S-SE-10](#) 3DMAG IC. The device can measure rotary motion in the horizontal and vertical planes, and measure linear motion side to side or front to back (Figure 6).

The A31315LOLATR-XY-S-SE-10 sensor provides designers the choice of ratiometric analog, PWM, or SAE J2716 single edge nibble transmission (SENT) output formats. It was developed to meet ISO 26262 ASIL B (single die, in a SOIC-8 package) and ASIL D (redundant dual die, in a TSSOP-14 package) capability in safety-related automotive systems.

Speed and direction: The [ATS19520LSNBTN-RSWHPYU](#) is a vibration-tolerant, differential Hall-effect transmission speed and direction gear tooth sensor, with models available for forward and reverse direction sensing (Figure 7).

The ISO 26262 ASIL B-rated sensor has integrated diagnostics and is suited for use in xEV drive trains. The three-pin, single-in-line package (SIP) includes an integrated back bias magnet to measure the speed and direction of rotating ferrous targets, and an integrated capacitor to ensure electromagnetic compatibility.
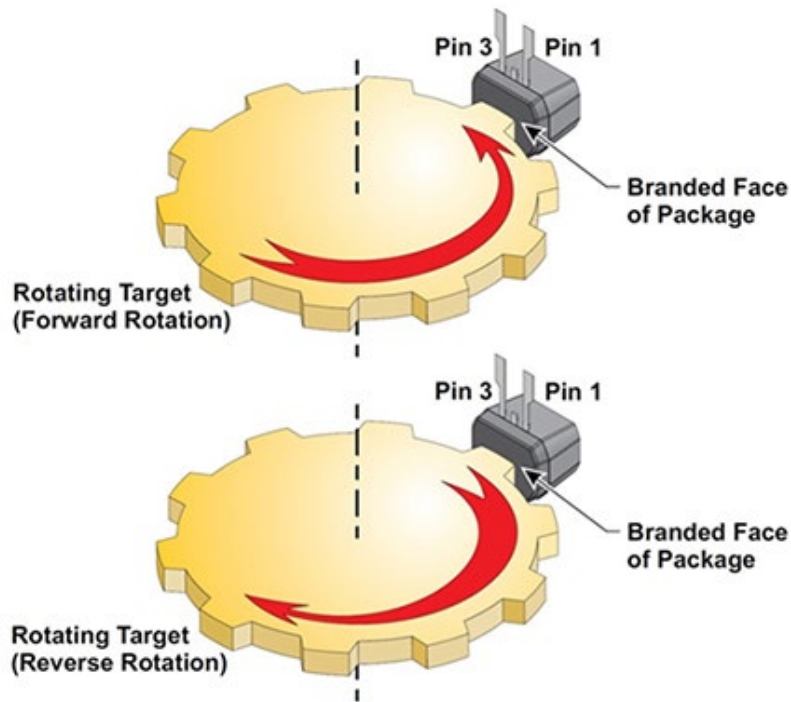

Figure 7: The shown "F" variant of the ATS19520 measures forward rotation when a gear tooth passes from Pin 1 to Pin 3 (top), and reverse rotation when a gear tooth passes from Pin 3 to Pin 1 (bottom). The "R" variant measures the rotation in the opposite directions. (Image source: Allegro MicroSystems)

Conclusion

Integrated sensorless FOC BLDC motor drives, along with current sensors, magnetic position sensors, and rotation sensors, are key components enabling the design of efficient and safe xEVs with greater driving ranges and lower carbon footprints. The use of FOC motor drives, in particular, enables the design of more efficient and quieter cooling systems with improved dynamic response for battery packs and traction inverters. For their part, compact, accurate, and energy-efficient sensors are critical to the development of xEVs that meet the reliability demands of advanced driver assistance systems and the functional safety requirements of ISO 26262.

Recommended reading

[Innovative Current Sensing for Vehicle Electrification](#)

[Effective Implementation of SiC Power Devices for Longer-Range Electric Vehicles](#)
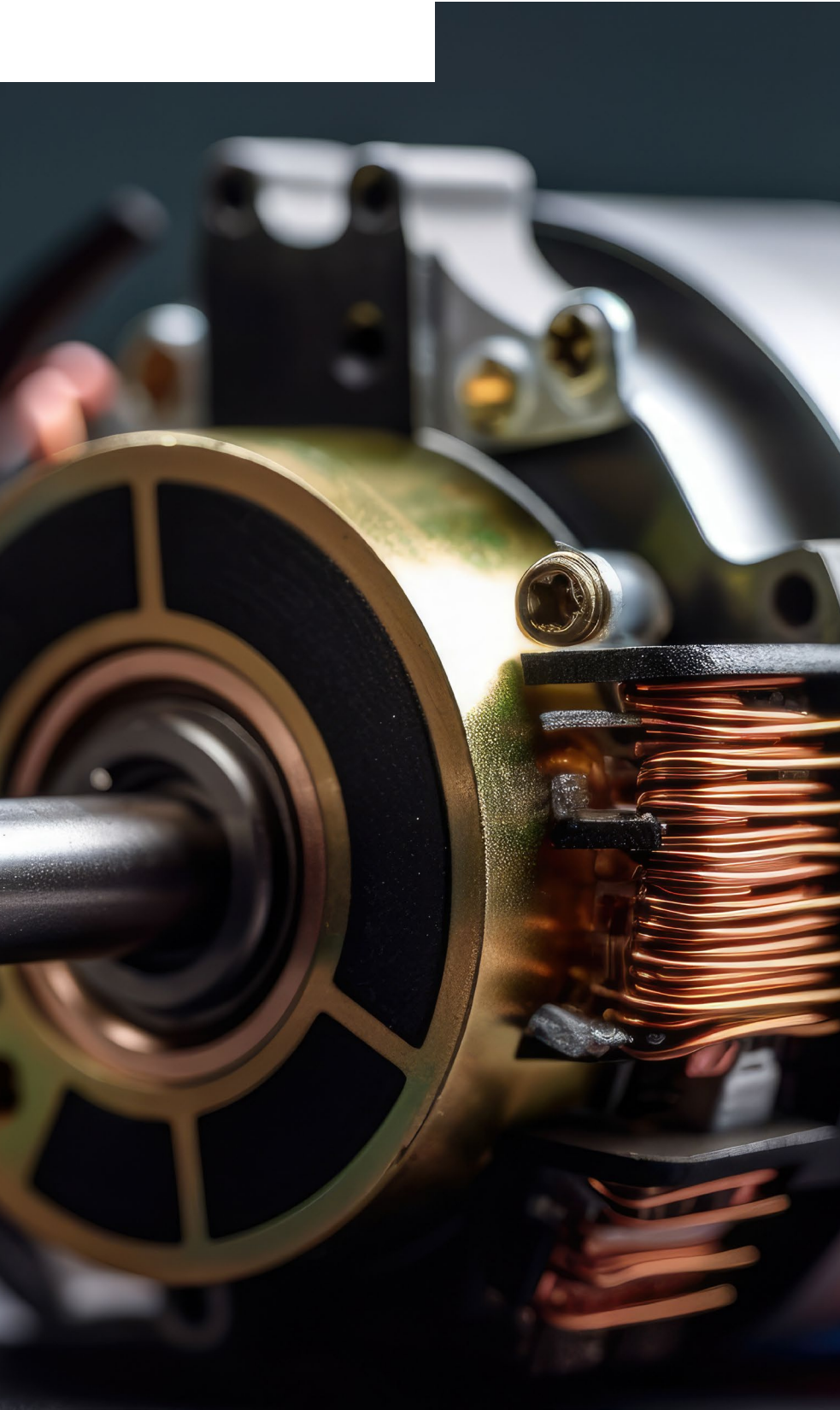
The basics of the controller area network (CAN bus) and its use in automotive applications
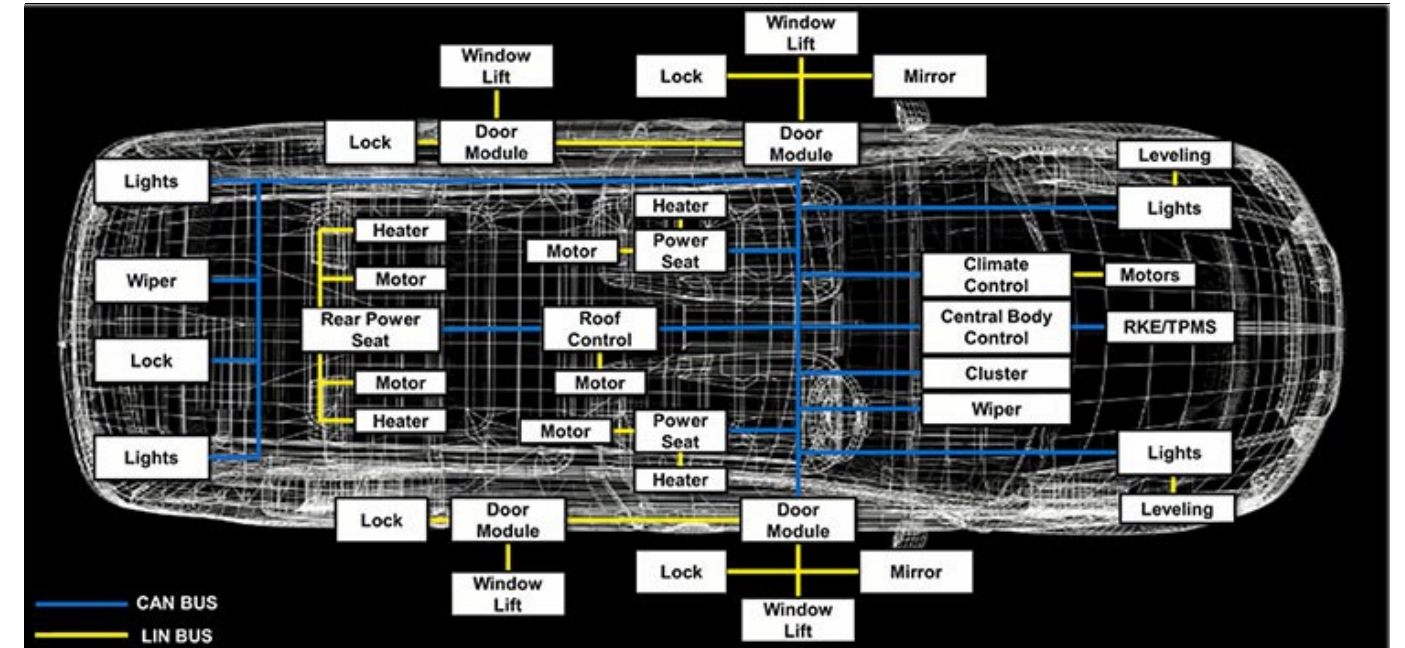
By Art Pini

Figure 1: The data bus connections in a typical vehicle implemented with CAN and LIN network elements. (Image source: Texas Instruments)

In-vehicle networks (IVNs) allow microcontrollers and engine control unit (ECU) processors to communicate with sensors, actuators, indicators, displays, and each other. The network bandwidth for IVNs depends on the function being supported. Typically basic body and comfort applications work fine with very low bus bandwidth, power-train and chassis applications require a little more bandwidth, safety features use medium bandwidth, infotainment applications use high bandwidth, while advanced driver assistance systems (ADAS) require very high bandwidth.

Also, IVNs can use multiple network architectures, each matched with a group of functional needs. One of the classic IVNs is the Controller Area Network or CAN bus. Let's take a look at it, and some example CAN bus transceivers from Texas Instruments.

CAN bus capabilities and structure

CAN has been around for about thirty years and continues to evolve. The classic CAN bus is described in the ISO11898 standard. It supports data rates of up to 1 megabit per second (Mbps) and handles medium bandwidth requirements.

The bus routing for a typical vehicle involves a great many connections. Figure 1 shows the large number of connections typical of modern vehicles. In this example, the CAN bus is linked to a lower-speed, local interconnect network (LIN) that operates at data rates of up to 20 kilobits per second (kbps), and is cost-effective for low-bandwidth needs.

The high cost and weight of a wiring harness in a vehicle means the implications of a

given network configuration must be given serious consideration upfront. The bus configuration in Figure 1 is very cost-effective and efficient. Rather than wire each sensor and actuator to a controller, the network routes multiple connections via simpler wired connections. The LIN bus uses a single wire for communications, and the CAN bus supports higher speeds using a single twisted pair.

As mentioned, the CAN bus, like all active networks, evolves continuously to meet the needs of the industry. CAN Flexible Data Rate (CAN FD) increases the data rate to 5 Mbps. The latest CAN standard is CAN Extra Long (CAN XL) and supports data rates of up to 10 Mbps or more. CAN FD and CAN XL are backward compatible with classic CAN.

The physical layer wiring for the CAN network consists of twisted pair wiring between CAN nodes, as shown in Figure 2.

The bus topology wiring of the CAN network requires 120 ohm (Ω) terminations at both ends of the bus to minimize reflections. Stubs—unterminated open connections—should be minimized. Bus rates depend on the CAN implementation and are affected by the length of the network. The longer the network, the lower the maximum data rate it can sustain. The 1 Mbps rated data rate is for a network length of 40 meters (m) or less.

$$V_D = CANH - CANL$$

Recessive when $V_D \leq 0.5$ V   **Dominant** when $V_D \geq 0.9$ V

A CAN compliant driver must produce at least 1.5 V across a typical 60 Ω load.

Figure 3: Shown are the differential signal definitions for the CAN bus CANH and CANL conductors. (Image source: Texas Instruments)

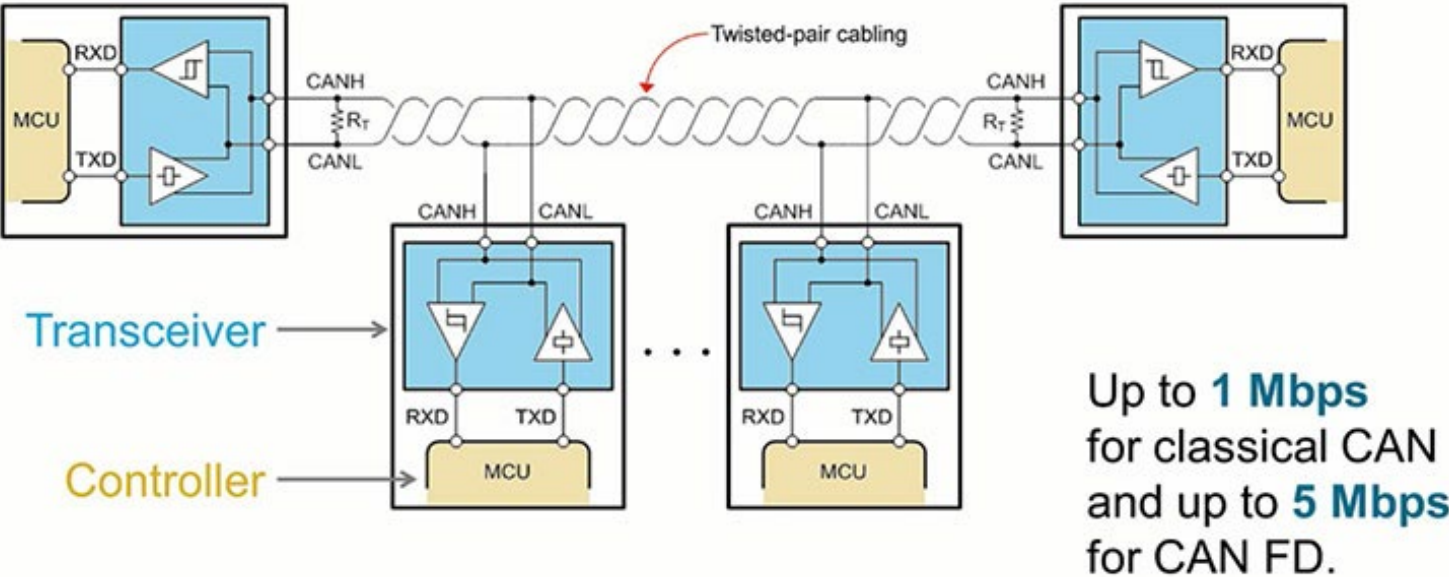Up to **1 Mbps** for classical CAN and up to **5 Mbps** for CAN FD.

Figure 2: The CAN bus uses terminated, twisted pair wiring, and nodes are drop connected. Each node has a CAN transceiver and a microcontroller unit (MCU) with a CAN controller function. (Image source: Texas Instruments)
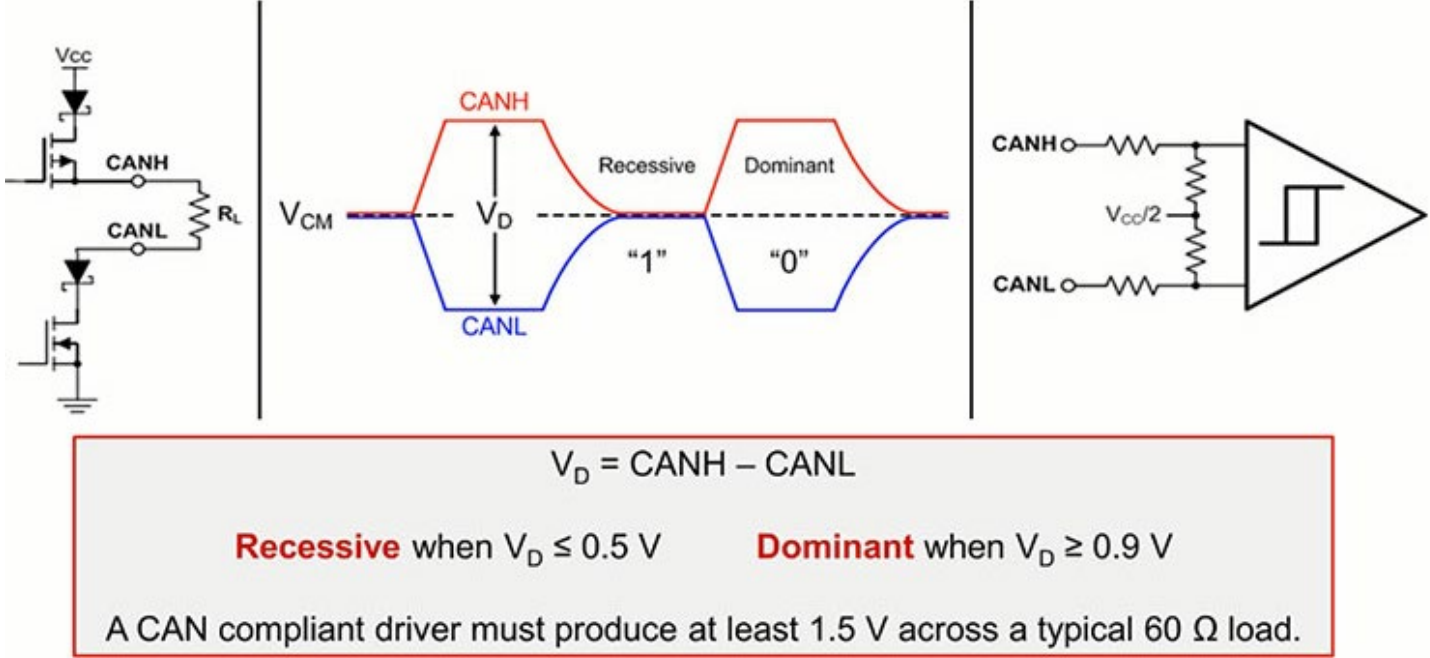
Communication across a CAN network relies on differential signaling using the two wires in the twisted pair designated CANH and CANL (Figure 3). The CAN transceiver driver is required to achieve a 1.5 volt differential signal across the 60 Ω differential load of the terminated twisted pair. The signal levels are referred to as dominant and recessive. The dominant or '1' level has a differential voltage level greater than or equal to 0.9 volts. The recessive or '0' level has a differential voltage of less than 0.5 volts.

The bus driver is capable of actively driving the bus to the dominant state, while the return to the recessive state depends on resistive discharge through the terminations. This accounts for the shorter rise time when transitioning from the recessive to the dominant state. It also allows a dominant bit to overwrite a recessive bit state. This feature is used for acknowledgment and bus arbitration.

The twisted pair transmission lines have a propagation delay of 5 nanoseconds per meter (ns/m). CAN

controllers are configured for the propagation delays of the network to which they are coupled, so this propagation delay information is needed to ensure correct bus arbitration and prioritization.

CAN transceivers, which physically drive the bus, are available in 8 pin and 14 pin versions. The Texas Instruments TCAN1042GDQ1 is an 8-pin version that supports CAN FD. Conveniently, Texas Instruments uses a common pin mapping for the top eight pins on both the 8 and 14 pin versions, allowing drop-in replacement.
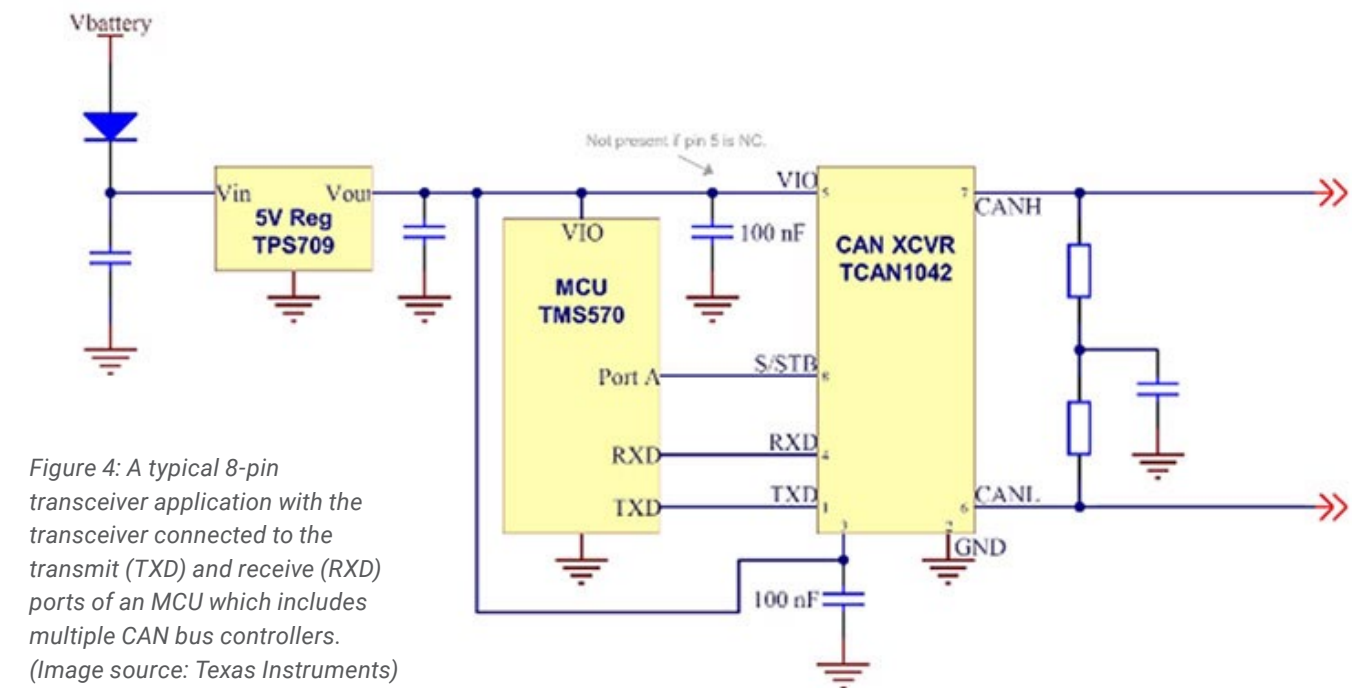
Figure 4: A typical 8-pin transceiver application with the transceiver connected to the transmit (TXD) and receive (RXD) ports of an MCU which includes multiple CAN bus controllers. (Image source: Texas Instruments)
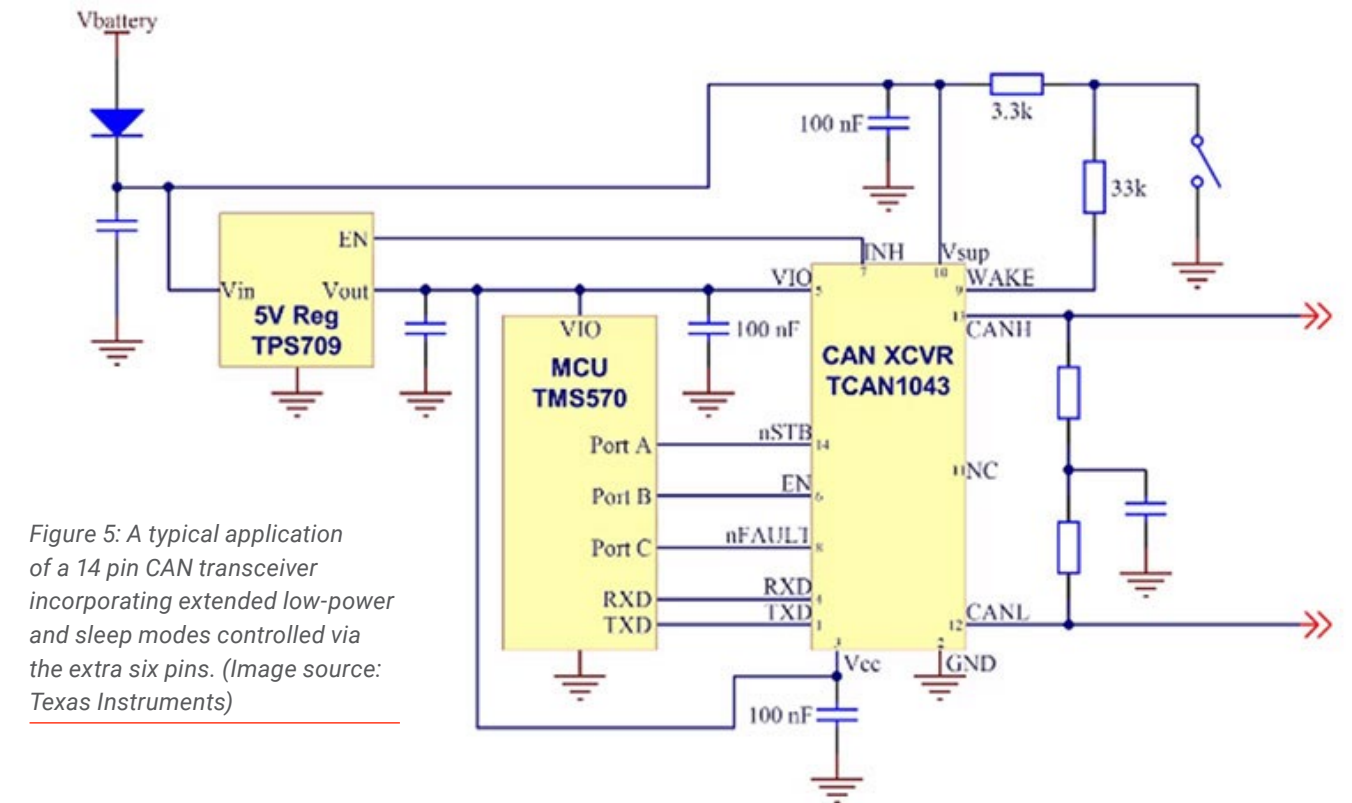

Figure 5: A typical application of a 14 pin CAN transceiver incorporating extended low-power and sleep modes controlled via the extra six pins. (Image source: Texas Instruments)

The transceiver is compatible with a Texas Instruments TMS5703137CGWTQEP microcontroller (MCU), which has three CAN controllers available (Figure 4).

14 pin CAN transceivers have additional functions, including auxiliary power buses and extended low-power and sleep modes.

The Texas Instruments TCAN1043GDRQ1 is a 14 pin CAN transceiver that supports full 5 Mbps operation under CAN FD. It is also compatible with the TMS5703137CGWTQEP MCU (Figure 5).

CAN protocol

The CAN bus follows a standardized protocol that allows the network to address data and commands where needed (Figure 6).

Between transmissions, the bus is in an idle state at the recessive voltage level. The start of the transmission frame (SOF) is marked by the transmission of a dominant bit. A message identifier in the next field is followed by a remote transmission request (RTR)—which indicates whether the frame contains data or is requesting data. These two fields are used to establish message priority and arbitrate access to the bus.

The Control Field contains the length of the following data field. The data field can have up to eight data bytes in classic CAN.

If data is being transmitted (data frame), then the data field is followed by the cyclic redundancy check (CRC) which is used to check for transmission errors. At this point, the driver puts the bus into a recessive state so the receiver can acknowledge (ACK) successful receipt by asserting a dominant state. The ACK bit is surrounded by delimiter bits on each side. After the ACK bit, the controller sends a seven-bit end-of-frame (EOF) message followed by a seven-bit interframe spacing, marking the minimum time before another frame can be transmitted.

Figure 6: The CAN protocol provides a structure for transferring data across the bus and verifying that it is received. It also provides error checking. (Image source: Texas Instruments)
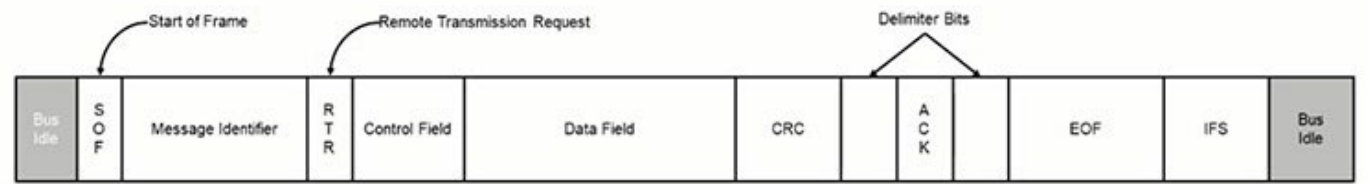
Start of Frame – A dominant bit begins the frame and initiates arbitration

Message Identifier – 11-bit identifier used for arbitration priority

Remote Transmission Request – Indicates whether this is a data or request frame

Control Field – Specifies the length of the data to be transmitted

Data Field – Up to eight bytes of data

CRC Sequence – 15-bit cyclic redundancy check

ACK – Acknowledges the CRC status of receiving nodes

End of Frame – Marks the end of data and remote frames

If the bit sequence contains five or more bits of the same state, then the controller will insert a stuff bit of the opposite state to ensure that there are sufficient edges in the signal to maintain synchronization. These stuff bits are removed by the receiver so that the data content is correct. After the CRC field, bit stuffing is deactivated to ensure that the ACK and EOF fields do not show stuff bits.

Differences between CAN and CAN FD

We already know that CAN FD operates at data rates of up to 5 Mbps compared to the 1 Mbps maximum data rate for CAN. This improvement is accomplished by increasing the data clock rate selectively; hence the name CAN FD (Figure 7).

In CAN FD, the clock rate during the data and CRC fields is increased so that twice as much data can be transmitted in the same period of time, or the same amount of data can be transmitted in half the time, giving CAN FD a greater bandwidth. The rest of the protocol timing remains the same. This arrangement is backward compatible, and CAN FD devices can operate in a CAN environment. Additionally, CAN FD supports data fields as large as 64 bytes compared to the eight-byte limit of CAN, which also increases the data rate.
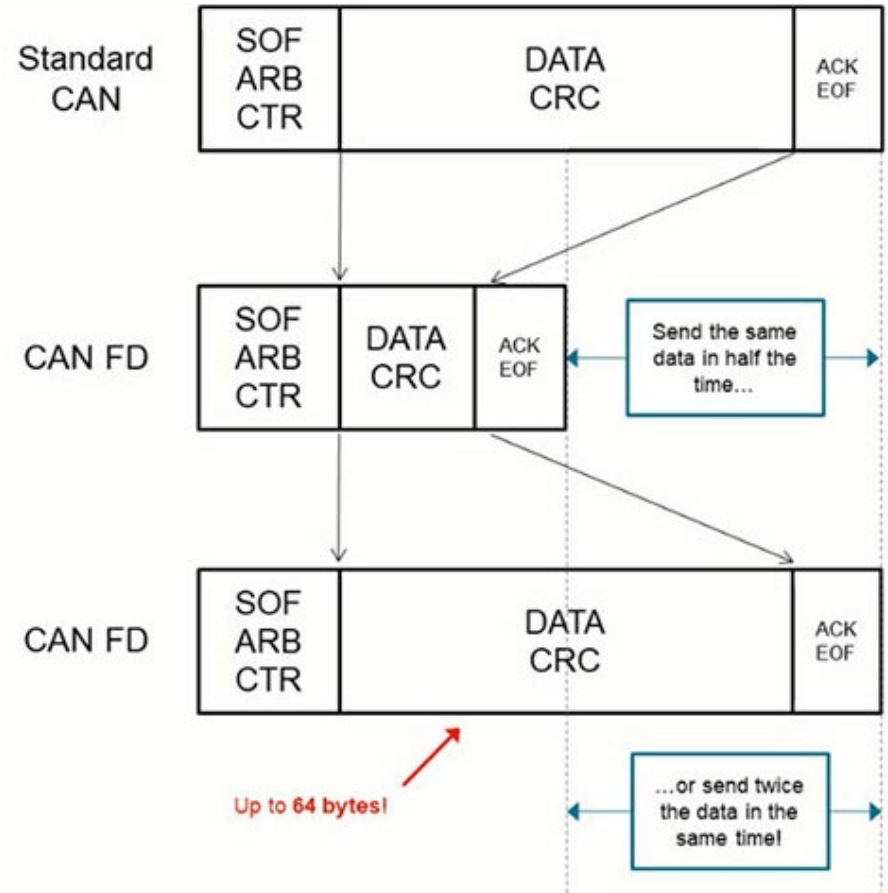

Figure 7: CAN FD uses a variable data rate in the data and CRC frames to increase the overall data rate of the transfer. (Image source: Texas Instruments)

What's ahead for CAN bus?

The high end of the in-vehicle network spectrum is occupied by 100BASE-T and 1000BASE-T Ethernet networks. There is quite a gap between lower-speed buses like CAN FD at 5 Mbps and these higher-speed buses. Currently, there are two contenders under development in the 10 Mbps space, namely 10BASE-T1S and CAN XL.

CAN XL increases the data rate and data payload size. The data payload length is increased to a maximum of 2048 bytes, accounting for the name "extra long." CAN XL still maintains backward compatibility with CAN and CAN FD for operation at lower speeds.

Conclusion

The CAN bus two-wire twisted pair interface has been around for many years and continues to grow to meet the expanding array of automobile connectivity requirements. It can be used by itself or to complement single-wire networks like LIN to minimize overall weight and cost. It is supported by a variety of classic and CAN FD transceivers from companies such as Texas Instruments.

You want to put how much current through your PCB?

By Mark Hughes
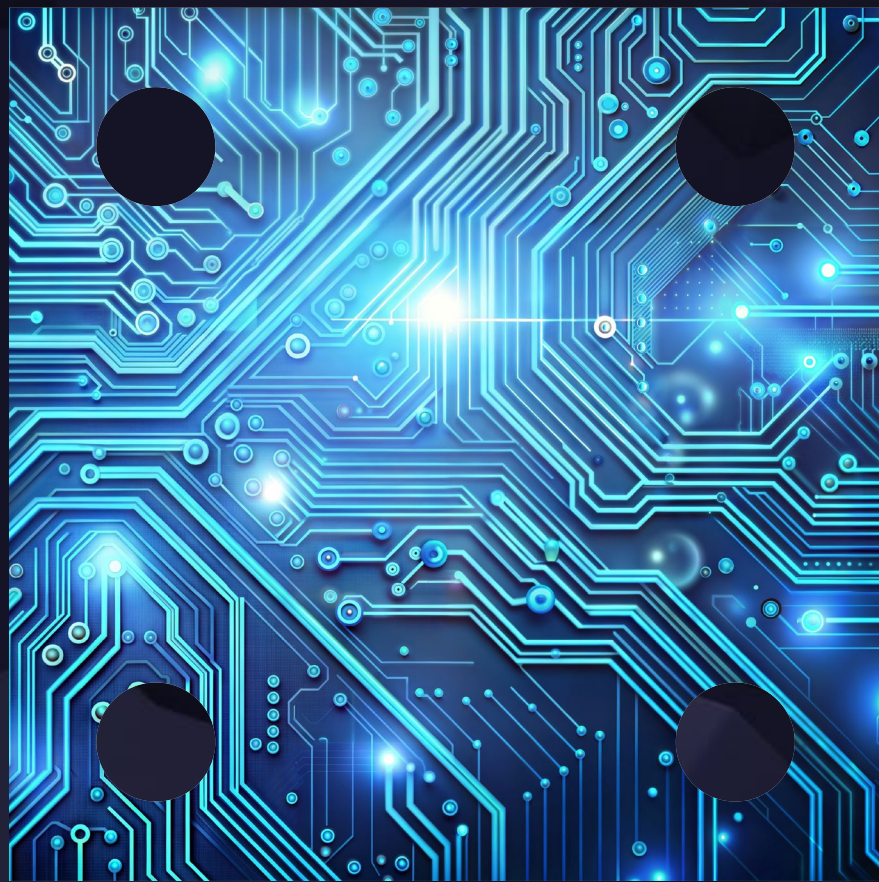
Introduction

A client once asked "What is wrong with my electronic speed controller design?" I quipped "it's two of the three parts of the fire triangle."

Before you release the magic smoke from your next design, take a moment to learn about high current and heavy copper PCB design best practices that apply to everything from Automotive, to FPGA to Servers, to Drones!

When I hear "High Currents," My mind always drifts towards one thing: Heavy Copper. Let's start our journey there!
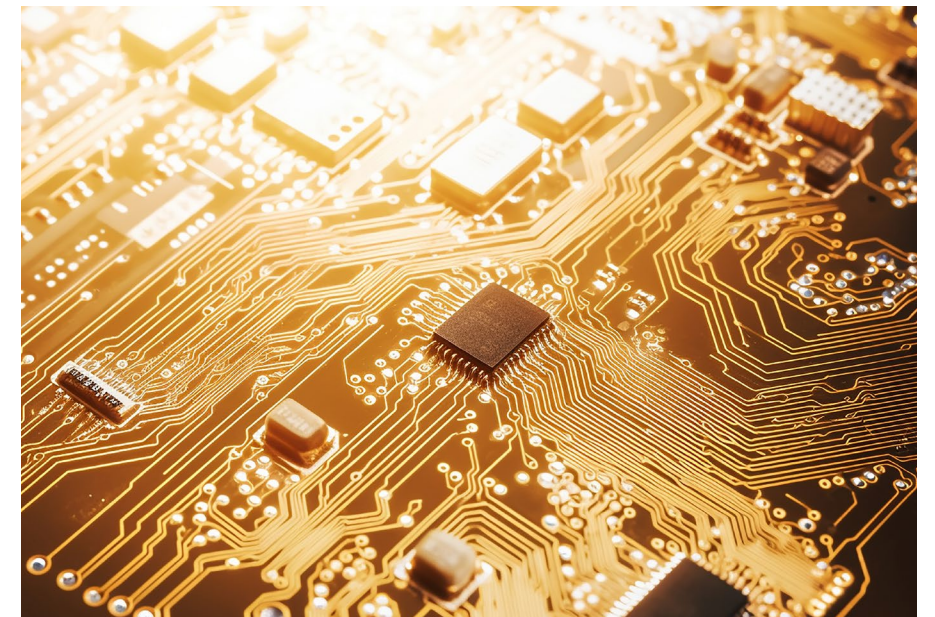
Heavy copper PCBs

Copper is second only to Silver in the electrical and thermal conductivity of metals. With greater workability and a much lower cost than silver, copper is the material of choice for PCB fabrication. Copper clad dielectrics and bare copper foil are readily available in a variety of factory-standard thicknesses ranging from 0.25 $[oz][ft]^{-2}$ to 4.0 $[oz][ft]^{-2}$. Thicker copper is available within a day from the warehouses of material suppliers like Insulectro, but aren't necessarily stocked on-hand inside PCB fabricator storerooms.

Once the density of copper exceeds 4 $[oz][ft]^{-2}$, fabricators and engineers tend to refer to these boards as *heavy copper* PCBs. There's a simple reason -- these PCBs might look normal, but are at least four times denser than you'd expect of a standard PCB, and feel unusually heavy in your hands. That extra heft is as unexpected as picking up a fully loaded suitcase you anticipated being empty.

The extra copper provides two benefits.

- The larger cross-sectional area provides reduced resistance, which means less heat generation in the traces for direct (DC) and low-frequency alternating currents (AC).

- The extra copper helps to conduct heat from higher-temperature to lower-temperature parts of your board. With a larger exposed surface area, it provides additional area for convective and radiative cooling.

The goal of using heavy copper is to limit any high temperature excursions that shorten the life of your PCB. But it's not all good news -- heavy copper has many drawbacks.

- Increased minimum trace and air-space width to accommodate increased copper-etching cut-back and compensation.

- Increased time in electroplating tanks to add copper traces and etching tanks to remove copper and create air-spaces.

- Increased difficulty in PCB assembly and rework stages.

- Increased weight

How much copper is too much copper? Or should I design to the standards?

Every time a client calls to ask me about using heavy copper on their next PCB design, the first question I always ask is "How did you determine your copper weight?" and nine times out of ten, they state "IPC-2221." With that little nugget of information, I can usually talk them out of hiring me within five minutes, by sharing what I'm about to share with you.

The best option you can use to determine your minimum copper trace width and thickness is a multiphysics or computational fluid dynamics simulation. But most electronics engineers lack the expertise, time, and most importantly, software licenses to fully simulate most designs.
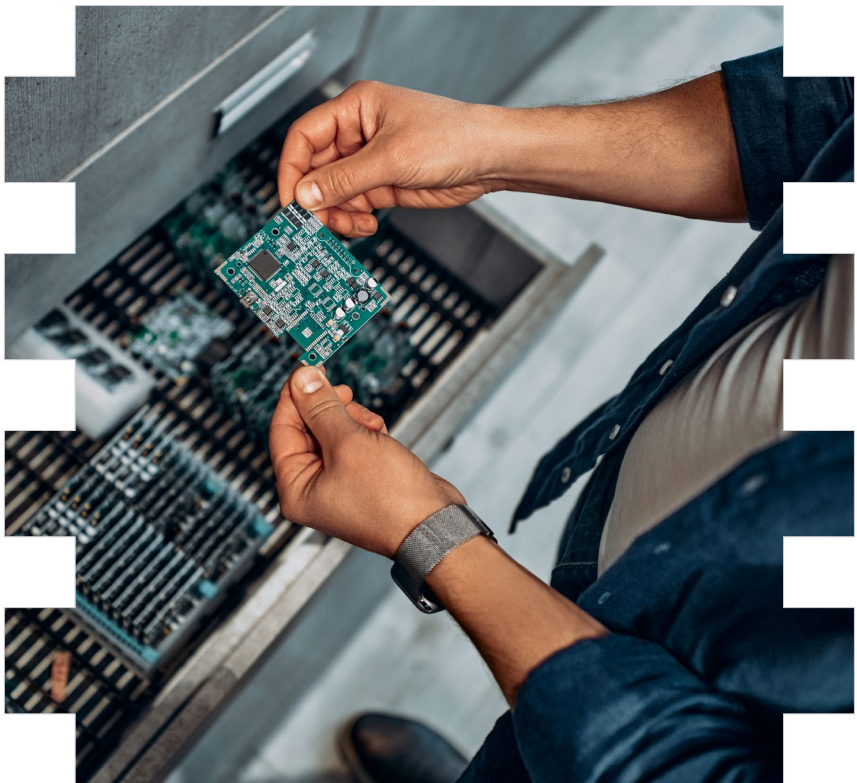
For years engineers used the data presented in IPC-2221 and were happy with the results because they were using so much copper, nothing ever overheated, so no one ever questioned the results. Many online calculators still use the equations in IPC-2221. As the saying goes: "Anyone can design a bridge that stands. It takes an engineer to design a bridge that barely stands."

The problem is that IPC-2221 is entirely too conservative and is based on incomplete research from six or seven decades ago

when PCBs were only one or two layers and made on materials such as phenolic resin.

Fortunately Mike Jouppi and the team responsible for the IPC-2152 standard discovered the faulted origins of the data, threw it out, and conducted fresh research using modern materials. To be clear, you should not use IPC-2221 trace width and thickness calculators in high current designs or your PCBs will be the size of pizza boxes.

Sierra Circuits has an excellent online calculator based on IPC-2152 at https://www.protoexpress.com/tools/trace-width-and-current-capacity-calculator/, but even IPC-2152 is based on a limited dataset and is more conservative than necessary. [Callout: The equations in IPC-2152 tell engineers to use more copper than they actually need. The equations in IPC-2221 tell engineers to use far more copper than they actually need.]

External Trace Width for Common Copper Weights at STP (△T=20° C)

$$\text{width}^{1.15} = \frac{215.3}{\Delta T} \frac{\text{current}^2}{\text{thickness}}$$

Trace Width [mils] vs. Current [Amps]

Copper Weight [Oz][Ft]$^{-2}$: 0.25, 0.5, 1.0, 2.0, 4.0
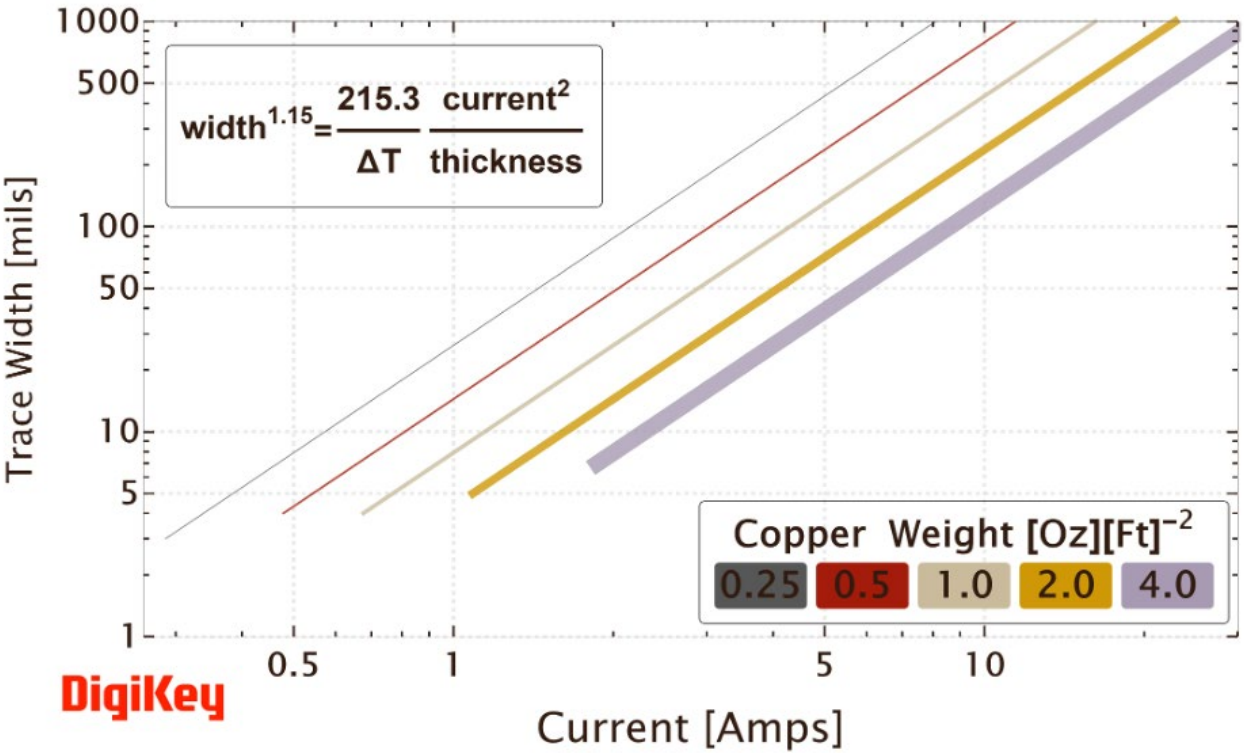
DigiKey

A quick interpretation of IPC-2152

The inner and outer layers of a PCB are made with different processes. In one single lamination stackup, the inner layers are etched into the board, then the outer layers are electroplated, and then copper is etched away from the entire board, leaving only the desired copper traces and land patterns behind. To ensure there is enough room for acid etching, there are minimum *trace* widths and air-space (*trace and space*) based on copper weight. For example, if you're using 0.5

$[oz][ft]^{-2}$ copper, the minimum advertised trace width is usually 3 mils and for 4 $[oz][ft]^{-2}$ copper, the minimum copper width is approximately 7 mils -- in both cases, the fabricators can produce thinner traces if asked, but we'll work with advertised minimums for now.

Trace and space minimums impact the size of components you can place on your board. Dies shrink every year, and when they do, package sizes often shrink with them. It doesn't take long for engineers to find themselves with parts that no longer fit on their old land-patterns.

This graph shows the minimum trace width required to maintain a temperature rise of no greater than 20° C at a given current in a variety of copper weights. To use this graph, assume your components can handle a 20° C rise, and on the horizontal axis find the current through your trace, then move vertically to find an acceptable copper weight and thickness. The graph uses equations derived from IPC-2152 data from the graphs by Douglas Brooks. It uses logarithmic axes and reimagined horizontal and vertical variable choices to produce graphs that look decidedly different from the graphs the IPC-2152 team created. You can download a complete assortment of these graphs in grams, ounces, mics, mils at https://aapcb.com/wp-content/uploads/2020/03/HeavyCopperGraphics.zip

According to IPC-2152, if you want the temperature of your board to rise no more than 20° C above ambient temperature, the minimum copper weight and trace width needed to conduct 5 amps of current in 4 $[oz][ft]^{-2}$ is approximately 50 mils. The minimum width of 2 $[oz][ft]^{-2}$ copper is ~100 mils. If you don't have 100 mils you can neck the trace down and hope for the best, or consider running the current over multiple layers of your

board and connecting the traces with multiple vias at the transition zones, remembering the decreased surface area will affect radiative and conductive cooling. Either way, ensure you've got a solid ground plane to help conduct the heat away from the warmer trace.

So what is an engineer to do?

Absent computer simulations or a hefty amount of design experience, your best bet is to stick to the IPC-2152 standard and have a little too much copper on your board. Paired with a solid ground plane, you should have no worries. Once fabricated and assembled, either put your board in its housing and attach thermoelectric probes to the surface of the board to track temperatures, or if there is no housing, paint the board in white-out fluid or Dr. Scholl's™ foot spray and use a thermal camera and see where the hot and cold spots are. Add copper in the area of the hot spots on the surface layers or on adjacent layers. Or perhaps add heat-sinks to the hot parts of the board whether on a component or directly to the board surface.

PCBA rework considerations

It is difficult to manually add or remove components on a heavy copper PCB without damaging the components. The reason is that

copper is such a good conductor of heat that it will immediately transfer and dissipate heat away from the area faster than a hot-air gun or soldering iron can transfer it into the components. That means rework technicians will tend to turn the temperature dials to their maximum setting. There are techniques to make rework possible, such as infrared underboard preheating, in combination with hot air guns and hot irons for rework, using solder removal alloy (Chip-quik) that lowers the melting temperature of the solder joint, and a few other tricks experienced rework technicians have hiding up their sleeves. The last heavy copper board I reworked required all of the techniques mentioned above, and in fact involved two additional hot-air guns and the assistance of an additional engineer to help hold everything. All that for a chip scale package I am too old to see without a microscope.

As an engineer you can do a few things to aid in rework, such as using the IPC-7351 nominal or maximum courtyard condition for component land patterns, this gives technicians an opportunity to easily deposit hot air or one of the thousands of soldering iron tips JBC offers right on the component without risk of damage to neighboring components. Another useful tip is to use thermal reliefs on

component pads. There will still be plenty of thermal and electrical conductivity, but the slight reduction in conductivity might be just enough to allow a technician to put enough heat into the solder to rework your board.

Your PCB assembly house will develop a custom solder heating profile for your board, but it will undoubtedly involve extra time in the reflow oven, which has the potential to damage sensitive parts. If you plan to use heavy copper, please work with your assembly partner early in the design process to avoid making a board that is so difficult to assemble that they decide to upcharge you.

Interposer boards

Every now and then I'll get a call from someone who wants to put a 0.35mm pitch ball-grid-array (BGA) on a heavy copper board, and they ask me how to do it, since the minimum trace width for 4 ounce copper is advertised to be 7 mils. If they make it past my first question of "are you still using IPC-2221 to select trace widths?" I always answer "It is not possible. There's not enough room to break out the pins of a micro-BGA given the minimum trace-widths and air-space requirements of heavy copper.
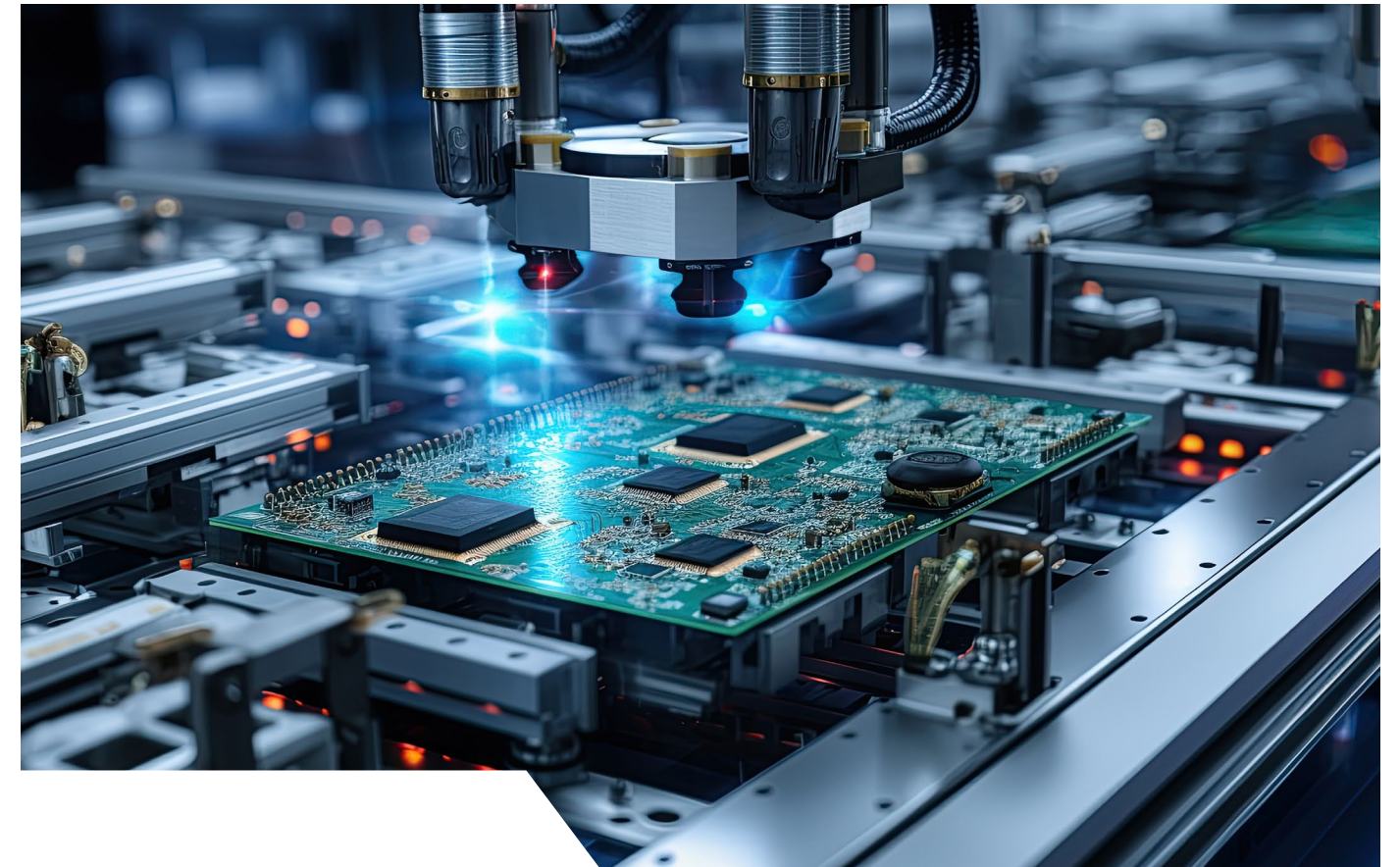
However, you can place the BGA on a small 0.5 ounce board, break out the pins there, and then attach the interposer board to the heavy copper board using vias."

But wait, there's more!

There is far more to know about working with heavy copper than I can write about in 2000 words. You'll have to do a bit more research on your own.

- For design best practices, I encourage you to find internet resources (webinars, papers, etc.) written by Mike Jouppi. He is, in my mind, the ultimate

resource for practical answers to questions such as: "How many VIAs do I need to transfer x Watts of heat?", "What is the difference in heat dissipation between outer and inner layers?", and more.

- Douglas Brooks has a book "PCB Design Guide to Vias and Trace Currents and Temperatures" some might find enlightening. His website also offers many of the pdf chapters of the book for free.

Take a photo of your next heavy copper pcb and tag Digikey, I can't wait to see what you're working on!

The parts we sell
help get you there safely

Today's cutting-edge vehicles can contain hundreds of sensors for systems that keep you comfortable, entertained, informed, and most importantly, safe.

The sensors we sell help engineers create these systems, but helping you enjoy your journey safely is what really drives us.

Find sensors for any application at digikey.com

DigiKey

we get technical

ECIA MEMBER
Supporting The Authorized Channel